Redox Biology 67 (2023) 102907

Contents lists available at ScienceDirect

Redox Biology

journal homepage: www.elsevier.com/locate/redox

Voltage-dependent anion channel 1 (VDAC1) overexpression alleviates cardiac fibroblast activation in cardiac fibrosis via regulating fatty acid metabolism

Geer Tian [a,1], Junteng Zhou [b,1], Yue Quan [a], Qihang Kong [a], Junli Li [a], Yanguo Xin [a], Wenchao Wu [a], Xiaoqiang Tang [c,d,e,**], Xiaojing Liu [a,*]

[a] Department of Cardiology and Laboratory of Cardiovascular Diseases, West China Hospital, Sichuan University, Chengdu, 610041, PR China
[b] Health Management Center, General Practice Medical Center, West China Hospital, Sichuan University, Chengdu, 610041, China
[c] Key Laboratory of Birth Defects and Related Diseases of Women and Children of MOE, State Key Laboratory of Biotherapy, West China Second University Hospital, Sichuan University, No.17 People's South Road, Chengdu, Sichuan, 610041, China
[d] National Health Commission Key Laboratory of Chronobiology, Sichuan University, No.17 People's South Road, Chengdu, Sichuan, 610041, China
[e] Development and Related Diseases of Women and Children, Key Laboratory of Sichuan Province, West China Second University Hospital, Sichuan University, No.17 People's South Road, Chengdu, Sichuan, 610041, China

ARTICLE INFO

Keywords:
Cardiac fibrosis
Cardiac fibroblasts
Voltage-dependent anion channel 1 (VDAC1)
Fatty acid metabolism

ABSTRACT

Cardiac fibrosis is characterized by the excessive deposition of extracellular matrix in the myocardium with cardiac fibroblast activation, leading to chronic cardiac remodeling and dysfunction. However, little is known about metabolic alterations in fibroblasts during cardiac fibrosis, and there is a lack of pharmaceutical treatments that target metabolic dysregulation. Here, we provided evidence that fatty acid β-oxidation (FAO) dysregulation contributes to fibroblast activation and cardiac fibrosis. With transcriptome, metabolome, and functional assays, we demonstrated that FAO was downregulated during fibroblast activation and cardiac fibrosis, and that perturbation of FAO reversely affected the fibroblast-to-myofibroblast transition. The decrease in FAO may be attributed to reduced long-chain fatty acid (LCFA) uptake. Voltage-dependent anion channel 1 (VDAC1), the main gatekeeper of the outer mitochondrial membrane (OMM), serves as the transporter of LCFA into the mitochondria for further utilization and has been shown to be decreased in myofibroblasts. *In vitro*, the addition of exogenous VDAC1 was shown to ameliorate cardiac fibroblast activation initiated by transforming growth factor beta 1 (TGF-β1) stimuli, and silencing of VDAC1 displayed the opposite effect. A mechanistic study revealed that VDAC1 exerts a protective effect by regulating LCFA uptake into the mitochondria, which is impaired by an inhibitor of carnitine palmitoyltransferase 1A. *In vivo*, AAV9-mediated overexpression of VDAC1 in myofibroblasts significantly alleviated transverse aortic constriction (TAC)-induced cardiac fibrosis and rescued cardiac function in mice. Finally, we treated mice with the VDAC1-derived R-Tf-D-LP4 peptide, and the results showed that R-Tf-D-LP4 prevented TAC-induced cardiac fibrosis and dysfunction in mice. In conclusion, this study provides evidence that VDAC1 maintains FAO metabolism in cardiac fibroblasts to repress fibroblast activation and cardiac fibrosis and suggests that the VDAC1 peptide is a promising drug for rescuing fibroblast metabolism and repressing cardiac fibrosis.

1. Introduction

Cardiac fibrosis is a common pathological process that occurs in response to acute or chronic stimuli, such as myocardial infarction, hypertension, and neurohumoral factor activation [1,2]. The main manifestations of fibrotic heart are cardiomyocyte hypertrophy and

* Corresponding author. Laboratory of Cardiovascular Diseases, West China Hospital, Sichuan University, Chengdu, Sichuan Province, 610041, PR China.
** Corresponding author. Key Laboratory of Birth Defects and Related Diseases of Women and Children of MOE, State Key Laboratory of Biotherapy, West China Second University Hospital, Sichuan University, No.17 People's South Road, Chengdu, Sichuan, 610041, PR China.
E-mail addresses: tangxiaoqiang@scu.edu.cn (X. Tang), liuxq@scu.edu.cn (X. Liu).
[1] Drs. Tian and Zhou contributed equally to this work.

https://doi.org/10.1016/j.redox.2023.102907
Received 4 September 2023; Received in revised form 23 September 2023; Accepted 26 September 2023
Available online 26 September 2023

phenotypic switching of cardiac fibroblasts. Excessive proliferation and activation of cardiac fibroblasts (CFs) lead to the deposition of the extracellular matrix, increasing the stiffness of the cardiac tissue matrix and dysregulation of myocardial contraction [2–5]. Eventually, the deposited extracellular matrix (ECM) impairs the systolic and diastolic functions of the heart. The activation of cardiac fibroblasts not only reflects myocardial cell injury but is also directly involved in the pathogenesis of myocardial dysfunction [6]. The metabolism pattern switch might play a critical role in cardiac fibroblast activation [7,8]. However, the underlying mechanism remains unclear.

Emerging evidence has revealed that metabolic remodeling initiates cardiac fibroblast activation and differentiation [9]. Fatty acid β-oxidation (FAO), especially long-chain fatty acid (LCFA) β-oxidation is considered the main source of energy under physiological conditions. However, glycolysis is the preferred metabolic pathway in the cardiac tissues under hypoxic conditions in heart failure. In pressure overload-induced cardiac hypertrophy, LCFA β-oxidation is impaired in cardiomyocytes [10]. However, the role of LCFA β-oxidation during the process of cardiac fibroblast activation remains unclear. Carnitine O-palmitoyltransferase 1a (CPT1a), the key enzyme in carnitine-dependent transport across the mitochondria is located in the outer membrane, and regulates the LCFA β-oxidation by promoting mitochondrial uptake. CPT1b haplodeficiency aggravates cardiac dysfunction when transverse aortic constriction (TAC) was performed in mice [11]. However, little is known regarding its role in CF metabolic switching and activation.

Mitochondria influence cell fate via energy supply, lipid homeostasis, and reactive oxygen species (ROS) generation. As one of the most abundant proteins in the outer mitochondrial membrane (OMM), voltage-dependent anion channel 1 (VDAC1) serves as a mitochondrial gatekeeper, regulating metabolic and energetic crosstalk between the mitochondria and cytoplasm [12–16]. VDAC1 functions as a two-way channel for ion exchange or short-sized metabolite intermediates, including ATP, glutamate, succinate, and pyruvate. A previous study reported that a CPT1B–P295A mutant constitutively binds to VDAC and rescues LCFA metabolism in PHD2/3-deficient cardiomyocytes, wherein complex formation rescues fatty acid metabolism [17]. Additionally, the VDAC1-based peptide R-Tf-D-LP4 arrests steatosis and NASH progression by affecting lipid metabolism and increasing the expression of enzymes and factors associated with fatty acid transport to the mitochondria [18]. However, the role of VDAC1 in pressure overload-induced CF activation and cardiac fibrosis remains unclear.

Here, we combined the RNA-sequencing and LC-MS/MS assay to analyze fatty acid metabolic alterations during cardiac fibroblast transdifferentiation (FMT) to myofibroblasts induced by TGF-β1 stimulation. During FMT, fatty acid degradation is downregulated and fatty acid transmembrane transport is inhibited. In addition, the elevated concentrations of LCFA with downregulated FAO in CFs may further contribute to excessive oxidative stress during FMT. We hypothesized that VDAC1 plays a doorkeeper role in regulating LCFA entry into mitochondria and that manipulating VDAC1 might alleviate the excessive activation of CFs by alleviating FAO disorders. Additionally, we administered pressure-overloaded mice with a VDAC1-derived R-Tf-D-LP4 peptide, which improved cardiac fibrosis *in vivo*. These findings demonstrate the importance of targeting fatty acid metabolism during fibroblast activation to alleviate cardiac fibrosis and suggest that VDAC1 may be a promising target.

2. Materials and methods

2.1. Study approvals and cardiac fibrosis model

Male C57BL/6 mice (6 weeks, 18–22 g) were procured from the Experimental Animal Tech Co. of Weitonglihua (Beijing, China). Transverse aortic constriction (TAC) surgery is widely performed to create models of cardiac fibrosis caused by induced pressure overload [3–5]. For surgery, mice were anesthetized using isoflurane (3% for induction and 1% for maintenance). The chest was then shaved and cleaned with alcohol. The mice were then intubated using PE 90 tubing in the supine position for mechanical ventilation with a tidal volume of 200 μl for a 20 g mouse and a respiratory rate of 130 breaths per minute. The chest was opened through a transverse incision and the aortic arch was exposed. A chest retractor was used to maintain the view. The aortic arch was constricted with a 5-0 silk suture tied around a 27-gauge blunt needle, which was removed after constriction. Sham-operated mice received a similar surgical treatment without ligation. Four weeks after TAC, echocardiography was performed on all mice to evaluate cardiac function. Then the mice were sacrificed, and their hearts were excised and snap-frozen in liquid nitrogen at −80 °C for further experiments. Animal experiments were approved by the Animal Ethics Committee of West China Hospital, Sichuan University (ethics number: 2018162A).

2.2. VDAC-derived R-Tf-D-LP4 peptide synthesis and injection

The R-Tf-D-LP4 peptide (KWTWKNSNGATWALNVATELKKEWTWSHRPYIAH, purity >95%) was purchased from Apeptide Bio-Technology Co., Ltd. (Shanghai, China) and has been reported in a previous study. The peptide was dissolved in DMSO and diluted in sterile saline for intravenous injection [18]. Mice with TAC were randomly subjected to an intratail vein injection of the R-Tf-D-LP4 peptide or control vehicle 3 days post-surgery. The peptide (in 100 μl of sterile saline) was intravenously administered every 3 days. A sham group was intravenously injected with 100 μl 0.2% DMSO in sterile saline. At the end of the experiment, mice were anesthetized with isoflurane for echocardiographic measurements.

2.3. Adeno-associated virus 9 (AAV9) construction and infection

AAV9 used in this study was purchased from Shanghai Genechem Co. Briefly, AAV9 carrying a *periostin* (*Postn*) promoter induced the overexpression of VDAC1 (AAV9-*Postn-Vdac1*). AAV9-*Postn-Vdac1* or AAV9-Postn-Ctrl (1×10^{11} v.g.) were injected intravenously into mice 7 days post-surgery. At the end of the experiment, mice were anesthetized with isoflurane for echocardiographic measurements.

2.4. Measurement of cardiac function by echocardiography

Echocardiographic measurements were performed using a Visual Sonics Vevo 3100 system (Visual Sonics, ON, Canada). The mice were anesthetized with isoflurane (2% for induction and 0.5% for maintenance). Chest hair was removed using a depilatory cream, and a layer of acoustic coupling gel was applied to the thorax. The heart rate, left ventricular (LV) end-diastolic and end-systolic chamber dimensions, and diastolic and systolic wall thicknesses were measured from the 2-D short-axis in M-mode at the mid-papillary muscle level. LV systolic function was determined by calculating the ejection fraction (EF) and fractional shortening (FS) using the above primary measurements and accompanying software.

2.5. Histological analyses

The mice were sacrificed, and freshly isolated heart tissues were fixed with 4% paraformaldehyde for 24 h at room temperature. Then the tissues were embedded in paraffin and sectioned at 5 μm for staining. The sections were stained with hematoxylin-eosin (HE) for routine histological examination. Collagen deposition was stained with Masson's trichrome (Solarbio Life Sciences, Beijing, China) and Sirius Red (Solarbio Life Sciences) according to the manufacturer's instructions. Stained sections were captured using a bright-field microscope (IX83, Olympus, Japan), and the degree of cardiac fibrosis was semi-quantitatively determined using National Institutes of Health (NIH) Image J software.

2.6. Isolation of cardiac fibroblasts of adult mice by flow cytometry sorting

At the end of the AAV infection experiment, mouse heart tissues were prepared as single-cell suspensions using the Multi tissue dissociation kit 2 (Mitenyi Biotec) and a gentle MACS Dissociator (Mitenyi Biotec), and the blood cells were lysed. The murine Fc block (BioLegend) was added to the cells to reduce nonspecific staining. Subsequently, the indicated antibodies (CD31-FITC, CD45-BV421, and MefSK4-APC) (BD Biosciences) at appropriate dilutions for membrane molecules were added and stained for 30 min at room temperature in the dark. The cells were washed with phosphate-buffered saline (PBS) and filtered through a 70 μm cell strainer before sorting by a multicolor flow cytometer (Beckman). Adult mouse cardiac fibroblasts gated from $CD45^{-}CF31^{-}MefSK4^{+}$ cell populations were collected for qPCR and Western blot analyses.

2.7. Flow cytometry analysis

For indirect intracellular staining of VDAC1 in $CD45^{-}$ $CF31^{-}$ $MefSK4^{+}$ cardiac fibroblasts, the cells were first fixed with 4% paraformaldehyde for 15 min, permeabilized with 0.5% Triton X-100 for 10 min at room temperature, and washed twice with PBS. An antibody against VDAC1 was added and incubated at room temperature for 1 h, followed by the addition of phycoerythrin (PE) goat anti-rabbit IgG (Cell Signaling Technology), staining for 1 h, and finally washing twice with PBS.

For flow cytometric analysis of primary CFs, cultured cells were harvested by digestion, centrifugation, and fixation with 4% paraformaldehyde for 15 min. CFs were suspended in staining buffer containing primary antibodies (anti-rabbit CD36) for 30 min at room temperature in the dark. After three washes, the CFs were incubated with secondary antibodies conjugated to FITC or PE.

Single-stained samples or UltraComp eBeads Compensation beads (Invitrogen) were used to adjust the compensation settings. Data were collected on a multicolor flow cytometer (BD Fortessa) and analyzed using the FlowJo software.

2.8. Immunofluorescence staining

At the end of the experiment, mouse hearts were harvested, fixed in 4% paraformaldehyde for 24 h, and embedded in paraffin. The paraffin tissues were sectioned at 5 μm, dewaxed in xylene and rehydrated with decreasing concentrations of alcohols at room temperature. The sections were then stained with primary antibodies. Alexa 488-conjugated goat anti-rabbit and Alex-555-conjugated goat anti-mouse antibodies were used as the secondary antibodies. The cross-sectional area of the cardiomyocytes was stained with wheat germ agglutinin (Alexa Fluor 488 conjugate WGA, 1:100, Vector Laboratories). Nuclei were stained with DAPI (1:2000, Invitrogen). Immunofluorescent staining of cardiac fibroblasts was performed as described previously [19]. The primary antibody used for incubation was *anti*-α-SMA (Abcam, ab124964, 1:200). Images were captured using an Olympus microscope (IX83, Japan). Fluorescence intensity was quantified using Image J software.

2.9. Isolation and culture of primary neonatal cardiac fibroblasts (CFs)

CFs were isolated as previously reported. Briefly, hearts from C57BL6 mice (birth, 0–3 days) were harvested and minced to 1 mm in cold PBS. The minced tissues were subsequently digested with a buffer containing trypsin (Gibco, USA) and collagenase II (Worthington, USA). The supernatant was then centrifuged to collect the cells. The cells were resuspended in DMEM supplemented with 10% FBS serum, plated in a culture flask, and incubated for approximately 60 min. The supernatants were discarded, and the flasks were replenished with fresh medium. The primary CFs were cultured at 37 °C in an incubator with 5% CO_2 and grown to 70–80% confluence. Cells in passages 2 and 3 were used for further experiments.

2.10. Treatments of CFs

The cells were incubated for 4–6 h in serum-free DMEM and then treated with TGF-β1 (10 ng/ml, Sino Biological Inc.) for 48 h to induce fibroblast activation and simulate fibrosis. For small-interference RNA (siRNA) transfection, CFs were seeded on plates, cultured to 70% confluence, and then transfected with *Vdac1* siRNA (*Vdac1*-siRNA), *Cpt1a* siRNA (*Cpt1a*-siRNA), or scrambled siRNA (NC-siRNA) (RiboBio, China) using Lipofectamine RNAiMax transfection reagent (Thermo Fisher Scientific, USA) for 24 h. For adenoviral infection, CFs were seeded onto plates, cultured to 70% confluence, and infected with VDAC1-overexpressing adenovirus (Ad-*Vdac1*) or control adenovirus (Ad-Ctrl) for 24 h. Adenoviruses were constructed by Hanbio (Shanghai, China).

Vdac1-siRNA: GCTGTGATGTGGACTTTGA
Cpt1a-siRNA: CCTGCATTCCTTCCCATTT

2.11. RT-qPCR

RT-qPCR was performed to detect gene expression. Briefly, total RNA was extracted using an RNA Extraction Kit (Tianmobio, China) following the manufacturer's instructions. The cDNA was synthesized using a reverse transcription (RT) kit (Toyobo, Japan). RT-qPCR was performed using gene-specific primers and detected using an SYBR Green Supermix kit (Bio-Rad, Hercules, CA, USA) on a CFX96 detection system (Bio-Rad). The primer sequences are shown in the Supplementary Material (Supplemental Table 1).

2.12. RNA-seq

Total CF RNA was isolated using an RNA extraction kit (Vazyme, RC112-01). The RNA quality and integrity were determined using a NanoDrop spectrophotometer (Thermo Fisher Scientific, USA). RNA from the control group and TGF-β1 treatment group were sequenced on the BGISEQ-500 NGS platform (BGI, Hong Kong) with subsequent mapping to the mouse reference genome (GRCm38) using HISAT2 software. RNA from CFs treated with *Cpt1a*-siRNA and NC-siRNA was sequenced using a HiSeq XTen sequencer (Illumina, San Diego, CA, USA). Fast QC was used to evaluate the quality of the sequenced data. All mRNA expression levels were quantified using the StringTie software. Raw sequencing data were deposited in a public dataset, SAR (accession numbers PRJNA838231 for CFs with vehicle and TGF-β1 treatment, and PRJNA992938 for CFs with *cpt1a*-siRNA and NC-siRNA transfection).

2.13. Bioinformatic analysis

Transcripts per kilobase million (TPM) eliminated the influence of gene length and sequencing discrepancies to enable a direct comparison of gene expression between samples. mRNAs with a false discovery rate (FDR) < 0.05, and log2 (fold change) > 1 were considered differentially expressed genes (DEGs) identified by DESeq2 [20]. Functional enrichment analyses, including Gene Ontology (GO) and Kyoto Encyclopedia of Genes and Genomes (KEGG), were used to identify DEGs that were significantly enriched in GO terms or metabolic pathways. Gene set variation analysis (GSVA) was performed to estimate changes in the pathways involved in fatty acid synthesis. The pathways in the control group and TGF-β1 treatment group were based on the signal value of the gene and the pathway where the gene is located. The enrichment score value of each sample was predicted using the signal value of the gene, and pathways with differential enrichment between the two groups were obtained. The R software package, GSVA, was downloaded from http://www.bioconductor.org. Pathways with FDR less than 0.05 were considered significantly enriched. The single-cell RNA-sequencing

database (GSE183852) of dilated cardiomyopathy (DCM) patients was analyzed to identify fatty acid metabolism-related alterations in cardiac fibroblast clusters. Unsupervised clustering of single cells was isolated from DCM patients using Uniform Manifold Approximation and Projection (UMAP) Projection. Gene sets of fatty acid-related pathways in cardiac fibroblasts from donors and patients with DCM were scored using the Ucell R package.

2.14. Sample preparation and LC-MS/MS analysis

Free long-chain fatty acids (LCFAs) and middle-chain fatty acids (MCFAs) from CFs after stimulation with TGF-β1 were analyzed by LC-MS/MS. The LC-MS/MS detection and analysis were performed by Metabo-Profile Biotechnology Co., Ltd. (Shanghai, China). For targeted analysis, cardiac fibroblast samples were collected according to published methods and the manufacturer's instructions [21]. Briefly, primary CFs were cultured and stimulated with TGF-β1 for 24 h. Then the cells were digested and harvested in a microcentrifuge tube and mixed with 10 per-chilled zirconium oxide beads and 20 μl of deionized water. Next, the sample was homogenized (3 min), and an internal standard was added to extract the metabolites. The sample was homogenized for another 3 min and centrifuged at 18000×*g* for 15 min. The supernatant was collected and added to a 96-well plate for further experiments, which were performed using a Biomek 4000 workstation (Beckman, USA). The plate was sealed after adding derivative reagents into each well, and derivatization was carried out at 30 °C for 60 min. Next, the plate was centrifuged at 4000 g and 4 °C for 30 min after adding methanal into each well. The supernatant was transferred to a 96-well plate and sealed for LC-MS/MS analysis.

An ultra-performance LC-MS/MS (UPLC−-MS/MS) system (ACQUITY UPLC-Xevo TQ-S, USA) was used to quantify the microbial metabolites. The separation was carried out on an ACQUITY UPLC BEH C18 column (2.1 × 100 mm, 1.7 μm), which was maintained at 40 °C and eluted at a flow rate of 0.40 ml/min. The mobile phase consisted of (A) water/acetonitrile (90:10, v/v) with 0.1% formic acid and (B) acetonitrile/IPA (70:30, v/v). The applied gradient elution program was as follows:0–2 min (15% B), 2–11 min (15–55% B), 11–11.2 min (55–100% B), 11.2–13 min (100% B), 13–13.2 min (100-15% B), and 13.2–16 min (15% B). The raw data files generated by UPLC−-MS/MS were processed using MassLynx software (v4.1; Waters, USA) to perform peak integration, calibration, and quantitation of each metabolite. The self-developed platform iMAP(v1.0, Metabo-Profile, China) was used for statistical analyses (PCA, OPLS-DA and pathway analysis, etc.).

2.15. Western blot analysis

Proteins were obtained from snap-frozen mouse heart tissues and cultured CFs according to a laboratory protocol using RIPA buffer (Beyotime, P0013B) with a protease inhibitor cocktail (MCE, HY-K0010) and a phosphatase inhibitor cocktail I (MCE, HY-K0021). Proteins were quantified using the BCA kit (Beyotime, P0012). Equal quantities of protein were separated by SDS−-PAGE and electrotransferred onto PVDF membranes (0.45 μm) (Millipore, IPFL00010). The membranes were blocked with Tris-buffered saline with 1% Tween 20 (TBST) containing 5% bovine serum albumin (BSA), and blots on membranes incubated with primary and secondary antibodies were detected using an enhanced chemiluminescence (ECL) kit (Bio-Rad, 1705060). Immunoblots were quantified using Image J software. The primary antibodies used in this study were against CPT1A (Proteintech, 15184-1-AP, 1:1000), p-AMPK (Huabio, ET1612-72, 1:1000), VDAC1 (Santa Cruz Biotechnology, sc-390996, 1:200; Proteintech, 55259-1-AP, 1:1000), CD36 (Huabio, ET1701-24, 1:1000), and GAPDH (Huabio, 60004-1-Ig, 1:1000). Image J software (National Institutes of Health) was used to quantify protein band intensities.

2.16. Cell EdU incorporation and immunofluorescence staining

An EdU staining kit (RiboBio, C10310) was used to detect CF proliferation, following the manufacturer's instructions. The CFs were digested and incubated with EdU, and the nuclei were stained with DAPI. Images were captured using an Olympus fluorescence microscope (IX83, Japan). The percentage of EdU-positive cells was calculated using Image J software.

2.17. Collagen cell contraction assay

A collagen contraction assay was performed to detect the contraction capability of CFs, following a previously reported method [22]. CFs were embedded in a complex of culture medium and collagen gel from the rat tail (Solarbio, #C8062) following the manufacturer's instructions. CFs were then administered different treatments, and the contraction capacity was measured from the gel image at the end of the experiment.

2.18. Cell fatty acid β-oxidation (FAO) detection

FAO activity in living cells was detected using FAOBlue (Funakoshi, # FDV-0033). FAOBlue is a coumarin dye containing a nonanoic acid (C9) protected by an acetoxymethyl ester and shows no fluorescence when excited at 405 nm before metabolization by FAO. FAOBlue can enter cells through direct penetration, convert to acyl-CoA, and be incorporated into the FAO pathway. After four FAO degradation cycles, the coumarin dye was released from propionic acid and showed strong blue fluorescence when excited at 405 nm [23]. The cardiac fibroblasts were stimulated with TGF-β1 for 24 h, and FAOBlue was added to the culture medium for an additional 2 h. Cells were then observed under a confocal microscope (LSM800, Zeiss, Germany) or collected for analysis using a flow cytometer (Fortessa, BD, USA).

2.19. Cell-scratching assay

Briefly, cardiac fibroblasts were plated in 6-well plates and treated with siRNA or adenovirus. The monolayer cells were then wounded with pipette tips, and images were obtained using a microscope. Meanwhile, the culture medium was replaced with a low serum culture medium, and TGF-β1 was added. At the end of the experiment, wound-healing images were obtained from approximately the same field. Representative images are shown.

2.20. Mitochondrial respiration assay

Mitochondrial respiration was detected by high-resolution respirometry (Oxygraph-2k, Oroboros, Innsbruck, Austria) at 37 °C. Primary CFs were isolated, cultured, and collected for the fatty acid oxidation (FAO) assay. In brief, the numbers of CFs in each group were counted and suspended in 0.5 mL of KHB buffer (111 mM NaCl, 4.7 mM KCl, 2 mM MgSO4, 1.2 mM Na2HPO4, 0.5 mM L-carnitine), which was added to the detection well for calibration. To evaluate the capacity of CFs to utilize long-chain fatty acids, 100 μM palmitic acid (PA) was used as the substrate for respiration, and 3 μM etomoxir was used to inhibit the cpt1a, the key rate-limiting enzyme of FAO.

2.21. Statistical analysis

Data are presented as the mean ± standard deviation (S.D). The significance of the differences was analyzed using an unpaired Student's *t*-test or one-way ANOVA with Bonferroni *post hoc* test and reported as $^{*}p < 0.05$, $^{**}p < 0.01$, or $^{***}p < 0.001$. GraphPad Prism 7 software was used for the analysis.

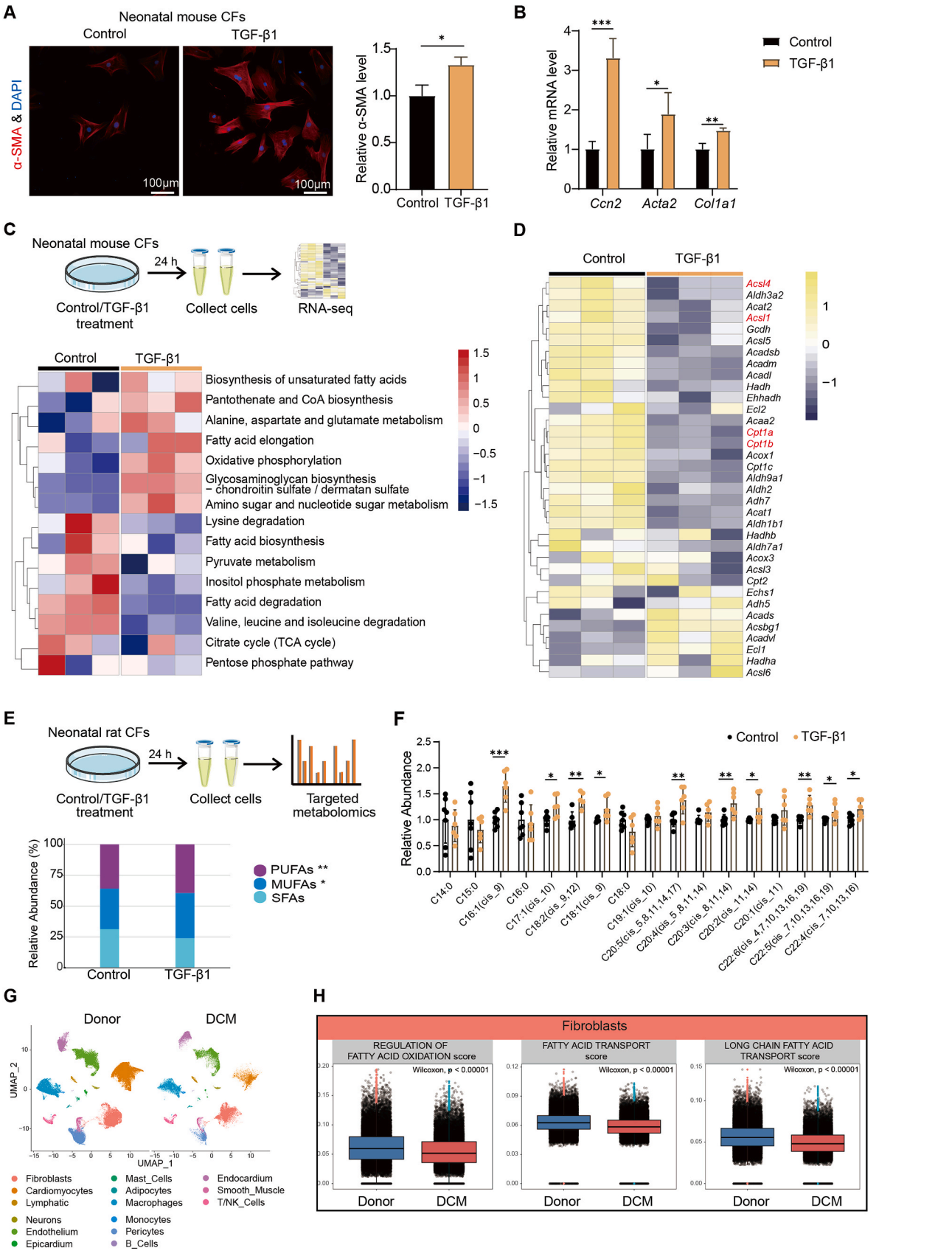

(caption on next page)

Fig. 1. Downregulation of FAO during cardiac fibroblast activation.
(A) Representative image showing α-SMA (red) and nuclei (blue) in cardiac fibroblasts with or without TGF-β1. (B) mRNA levels of fibrotic markers (*Ccn2, Acta2*, and *Col1a1*) are relative to the control (n = 3). (C) RNA sequencing and GSVA of primary cardiac fibroblasts obtained from mice to analyze the main metabolic alterations involved in fibroblast activation (n = 3). (D) The significant differentially expressed genes involved in fatty acid metabolism are listed, showing the downregulated expression of oxidative genes and upregulated expression of synthesis genes. (E) The free long-chain fatty acid (LCFA) concentrations of primary cardiac fibroblasts in SD rats were detected using LC-MS/MS. Polyunsaturated fatty acids (PUFAs) and monounsaturated fatty acids (MUFAs) accumulated in control fibroblasts or TGF-β1-treated fibroblasts (n = 6). (F) Selection of LCFAs measured using LC-MS/MS in control fibroblasts or TGF-β1-treated fibroblasts, fold change relative to the control group (n = 4–6). (G) Uniform Manifold Approximation and Projection (UMAP) showing unsupervised clustering of single cells isolated from dilated cardiomyopathy (DCM) patients. (H) Scoring of gene sets involved in fatty acid-related pathways in cardiac fibroblasts in donors and DCM patients using Ucell R package. The results are presented as the means ± S.D. $*p < 0.05$, $**p < 0.01$, $***p < 0.001$; Student's *t*-test. (For interpretation of the references to color in this figure legend, the reader is referred to the Web version of this article.)

3. Results

3.1. Fatty acid metabolism alterations during the activation of cardiac fibroblasts

To unravel distinct mRNA expression profiles in cardiac fibroblasts and myofibroblasts, we performed RNA sequencing (RNA-seq) on primary cardiac fibroblasts treated with TGF-β1 for 24 h. After 24 h of TGF-β1 stimulation, the fibrotic marker α-smooth muscle actin (α-SMA) was upregulated in cells, which revealed that the phenotype switched from fibroblasts to myofibroblasts (Fig. 1A). Meanwhile, mRNA expression of fibrotic markers, including *Ccn2, Acta2*, and *Col1al*, increased after TGF-β1 stimulation, as detected by real-time quantitative PCR (RT-qPCR) (Fig. 1B). To uncover the metabolic alterations in fibroblast activation, the main related KEGG metabolic processes were analyzed using gene set variation analysis (GSVA). The results revealed enhanced fatty acid elongation, decreased fatty acid biosynthesis, and decreased fatty acid degradation in cardiac myofibroblasts, suggesting downregulation of FAO and accumulation of LCFA (Fig. 1C). In addition, the heatmap showed the expression of fatty acid degradation-related genes, including *Cpt1a, Cpt1b*, and *Acsl1*, which were downregulated in TGF-β1-treated cardiac fibroblasts (Fig. 1D). To further determine the specific process that caused fatty acid degradation to decrease, we performed GSVA, focusing on the biological pathways related to fatty acid metabolism. These results demonstrate that fatty acid transmembrane transport may be a major factor (Supplemental Fig. 1A).

To further confirm the fatty acid alteration during CF activation, LC-MS/MS was performed to detect the concentration changes in intracellular free medium- and long-chain fatty acids in TGF-β1-treated cardiac fibroblasts. The proportions of polyunsaturated fatty acids (PUFAs) and monounsaturated fatty acids (MUFAs) were significantly increased in TGF-β1-treated CFs (Fig. 1E). Both PUFAs and MUFAs are long-chain fatty acids (LCFAs) with over 12 carbon atoms that are transferred into cells and are regulated by CD36 [24]. The results showed that LCFAs with a larger concentration were more abundant in TGF-β1-treated cardiac fibroblasts, including palmitoleic acid (C16:1), linoelaidic acid (C18:2), and eicosapentaenoic acid (C20:5) (Fig. 1F). The accumulation of fatty acids and downregulation of fatty acid degradation may induce cellular oxidative stress [25]. Then, the flow cytometry-based quantification of ROS displayed a significant increase in TGF-β1-treated cardiac fibroblasts compared with control (Supplemental Fig. 1B).

Furthermore, single-cell and single-nucleus sequencing data from non-diseased donors and dilated cardiomyopathy (DCM) patients were analyzed. After unsupervised clustering, integration, and differential expression analysis, the cell entities were validated by the expression of cell-specific marker genes and transcriptional signatures. Cell types identified in both snRNA-seq and scRNA-seq datasets included fibroblasts, endothelial cells, myeloid cells, smooth muscle cells, pericytes, T cells, natural killer (NK) cells, neurons, and B cells (Fig. 1G). The gene sets of fatty acid-related pathways in cardiac fibroblasts from donors and DCM patients were scored using the Ucell R package. The results indicated that cardiac fibroblasts of patients with DCM had lower scores for fatty acid oxidation, fatty acid transport, and long-chain fatty acid transport than those of the donors (Fig. 1H).

In summary, there is a downregulation of fatty acid degradation and excessive accumulation of LCFAs in TGF-β1-treated cardiac fibroblasts corresponding to the oxidative stress of myofibroblasts, which is supposedly due to the inhibition of fatty acid transmembrane transport.

3.2. Perturbation of FAO affects the fibroblast-to-myofibroblast transition

To illustrate the capacity alteration of FAO during fibroblast activation, we quantified FAO capacity using FAO-blue dye and the intensity of fluorescence was observed by confocal microscopy. The results showed that FAO was decreased in myofibroblasts (Fig. 2A). Then we detected the protein levels of enzymes involved in FAO and the results showed that the protein levels of CD36, p-AMPK and CPT1a were decreased in TGF-β1-treated cardiac fibroblasts (Fig. 2B). CPT1a is a critical enzyme for FAO, transferring the fatty acyl groups of acyl-CoA to carnitine to form acylcarnitine [26]. To demonstrate the role of metabolic changes in cardiac fibroblast activation, we inhibited FAO using the CPT1 inhibitor etomoxir or enhanced FAO using the AMPK agonist AICAR. The CFs were pretreated with etomoxir (final concentration of 4 μM, beyond which it would have off-target effects on mitochondrial respiration), and TGF-β1 was subsequently added. The results indicated that inhibition of CPT1a significantly enhanced the profibrotic capability of TGF-β1-treated CFs, as confirmed by α-SMA intensity, EdU staining, and collagen cell contraction assays (Fig. 2C&D and Supplemental Fig. 2A).

As an upstream regulator of CPT1a, AMPK is a pivotal enzyme that regulates FAO and cardiac fibrosis [27,28]. To further confirm the role of FAO in the cardiac fibroblast-to-myofibroblast transition, we used AICAR, an AMPK agonist, to stimulate FAO. The results showed that activation of AMPK significantly inhibited the fibroblast to myofibroblast transition of TGF-β1-treated CFs, as confirmed by α-SMA intensity, EdU staining, and collagen cell contraction assays (Supplemental Figs. 2B–D).

To elucidate the mechanism by which downregulation of FAO affects cardiac fibroblast activation, we silenced *Cpt1a* in cardiac fibroblasts by transfecting them with small interfering RNA (siRNA). The two groups transfected with *Cpt1a*-siRNA or negative control-siRNA (NC-siRNA) were clearly divided into two clusters by PCA (Supplemental Fig. 2E). We then detected typical markers of fibroblast activation, and the downregulated expression of *Postn, Acta2, Ccn2,* and *Col1a1* indicated that silencing *Cpt1a* promoted cardiac fibroblast activation (Fig. 2E). GO and KEGG analyses indicated that silencing *Cpt1a* affected fatty acid metabolic processes, oxidation, transport, and other pathways involved in fatty acid metabolism (Fig. 2F). A previous study indicated that CPT1a catalyzes the conversion of acyl-CoA into long-chain fatty acylcarnitine, depending on the protein complex on the outer membrane of the mitochondria (OMM) [29]. Because these pathways are related to mitochondrial proteins and function, we enriched the related GO pathways, including the mitochondrial protein-containing complex and mitochondrial matrix, using GSEA analysis (Fig. 2G). A Venn diagram was used to illustrate the distribution of genes in the mitochondrial protein-containing complex and matrix pathways (Fig. 2H). To identify the core genes involved in fatty acid metabolism, we showed the

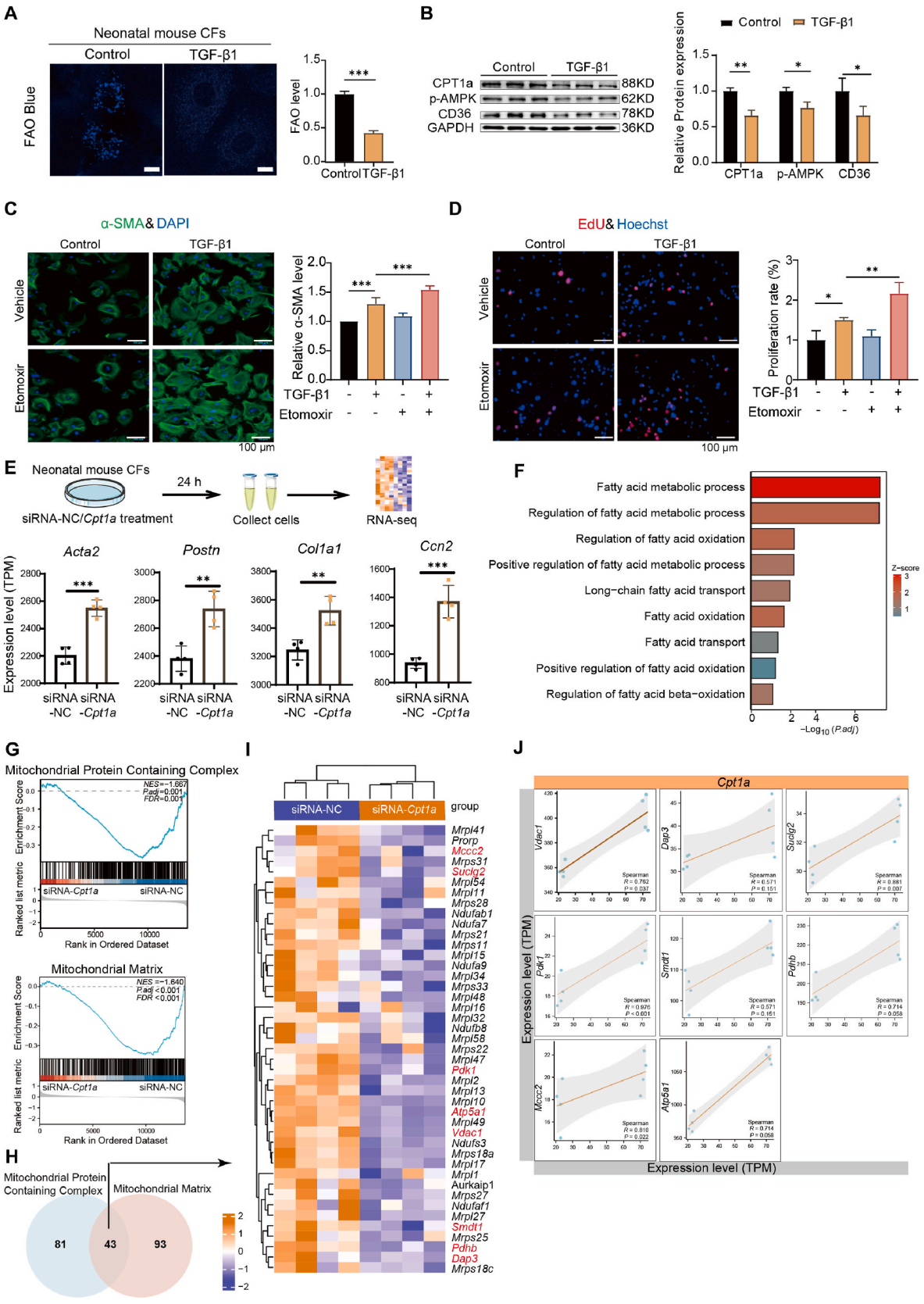

(caption on next page)

Fig. 2. Perturbation of FAO affects the fibroblast-to-myofibroblast transition.
(A) The capacity of FAO in primary mice cardiac fibroblasts (PMCFs) reflected by the intensity of fluorescence of the FAOblue dye, observed using confocal microscopy (n = 6). Bars represent 10 μm. (B) The protein levels of FAO-related enzymes, including CPT1a, p-AMPK, and CD36 (n = 3). (C) Representative image showing α-SMA (green) and nuclei (blue) in PMCFs with the indicated treatment for 24 h (n = 3). (D) Representative image of EdU staining, indicating the proliferation capacity of PMCFs with the indicated treatment for 24 h (n = 3). (E) RNA sequencing of PMCFs transfected with *Cpt1a*-siRNA or negative control-siRNA, and the mRNA expression (TPM) of typical fibrotic markers (*Acta2, Postn, Col1a1,* and *Ccn2*) of two groups (n = 4). (F) KEGG and GO analysis of the fatty acid-related pathway affected by *Cpt1a* silencing in PMCFs (n = 4). (G) Gene set enrichment analysis (GSEA) score of mitochondrial protein-containing complex of PMCFs treated with *Cpt1a*-siRNA and NC-siRNA (n = 4). (H) Venn diagram illustrating the distribution of genes in the two pathways involved in the synthesis of the mitochondrial protein-containing complex and mitochondrial matrix. (I) Heatmaps showing the expression pattern of forty-three genes intersected in the two pathways of mitochondrial protein-containing complex and mitochondrial matrix in PMCFs treated with *Cpt1a*-siRNA and NC-siRNA (n = 4). (J) Association analysis of expression of *Cpt1a* and genes picked from heat maps excepting the mitochondrial respiratory chain complex protein and mitochondrial ribosomal protein, including *MCC2, Suclg2, Vdac1, Pdk1, Atp5a1, Smdt1, Pdhb,* and *Dap3* (n = 4). The results are presented as the means ± S.D. *$p < 0.05$, **$p < 0.01$, ***$p < 0.001$; A and B, Student's *t*-test; C&D, One-way ANOVA with Bonferroni *post hoc* test. (For interpretation of the references to color in this figure legend, the reader is referred to the Web version of this article.)

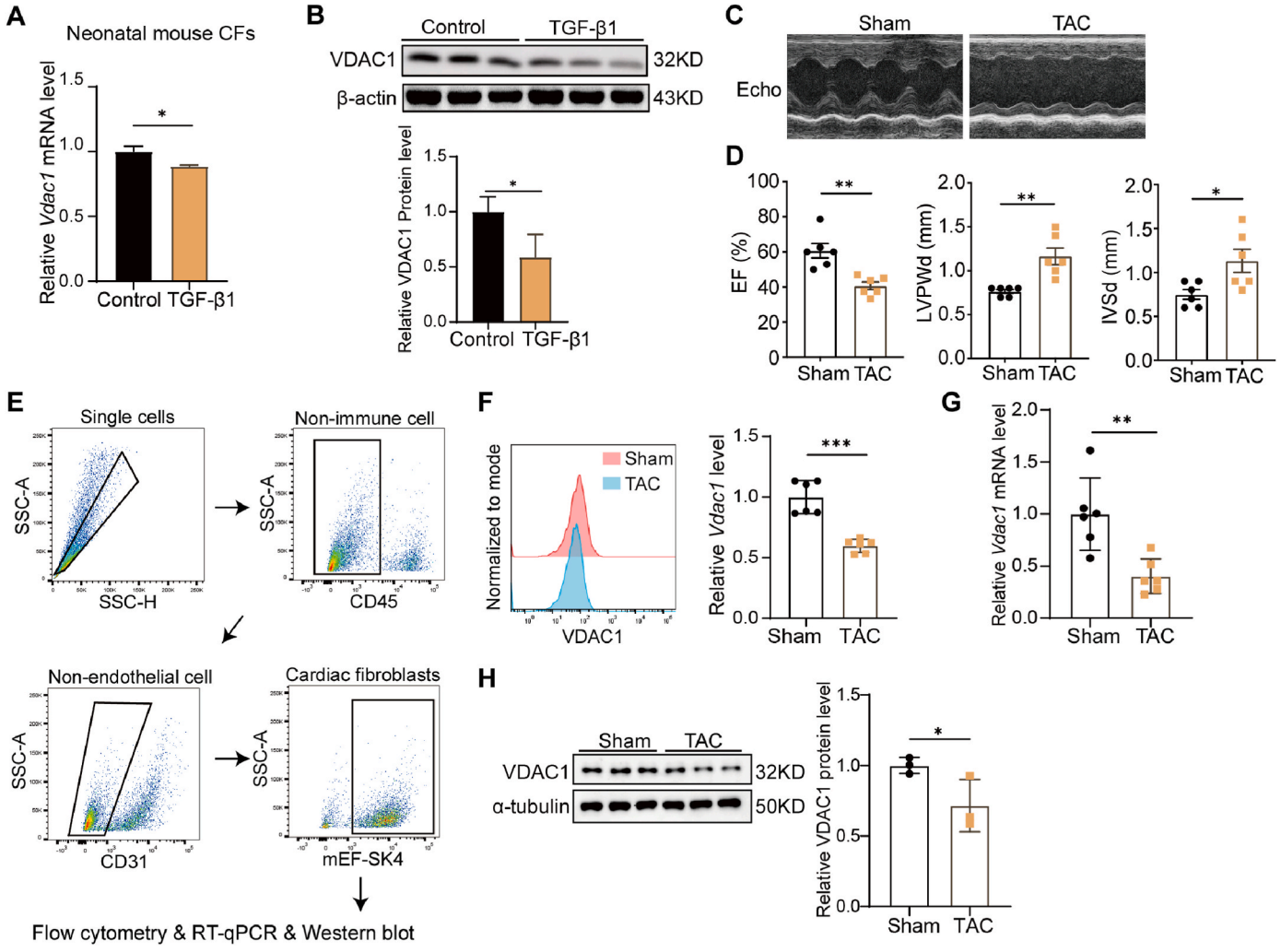

Fig. 3. VDAC1 is decreased in fibrotic cardiac tissues and TGF-β1-induced myofibroblasts.
(A) mRNA expression of *Vdac1* in cardiac fibroblasts with or without TGF-β1 treatment (n = 3). (B) Protein levels of VDAC1 in cardiac fibroblasts with and without TGF-β1 treatment (n = 3). (C) Representative images of echocardiography and hearts of mice in the Sham and TAC groups. (D) Echocardiographic parameters measured in mice 4 weeks after sham or TAC (n = 6). (E) Flow cytometry sorting panel of cardiac fibroblasts from mouse heart tissue after TAC. (F) VDAC1 levels in $CD45^{-}CD31^{-}mEF\text{-}SK4^{+}$ cardiac fibroblasts from mice in the Sham and TAC groups, as detected through flow cytometry. (G) The mRNA levels of *Vdac1* in $CD45^{-}CD31^{-}mEF\text{-}SK4^{+}$ cardiac fibroblasts from mice in the Sham and TAC groups as detected using RT-qPCR (n = 6). (H) Protein levels of VDAC1 in $CD45^{-}CD31^{-}mEF\text{-}SK4^{+}$ cardiac fibroblasts from mice in the sham and TAC groups as detected using western blotting (n = 3). The results are presented as the means ± S.D. *$p < 0.05$, **$p < 0.01$; Student's *t*-test. IVSd, interventricular septum in diastole; LVPWd, left ventricular posterior wall in diastole; EF, ejection fraction.

expression patterns of 43 genes that intersected in the mitochondrial protein-containing complex and mitochondrial matrix. We then analyzed the association between the expression of *Cpt1a* and genes selected from the heat maps, except for mitochondrial respiratory chain complex proteins and mitochondrial ribosomal proteins, including *MCC2*, *Suclg2*, *Vdac1*, *Pdk1*, *Atp5a1*, *Smdt1*, *Pdhb*, and *Dap3* (Fig. 2I). The association analysis results indicated that *Vdac1*, a channel protein that regulates the transport of fatty acids, had a high positive correlation with *Cpt1a* (R = 0.762, *P* = 0.037) (Fig. 2J).

Previous studies have reported that CPT1 can form a complex with

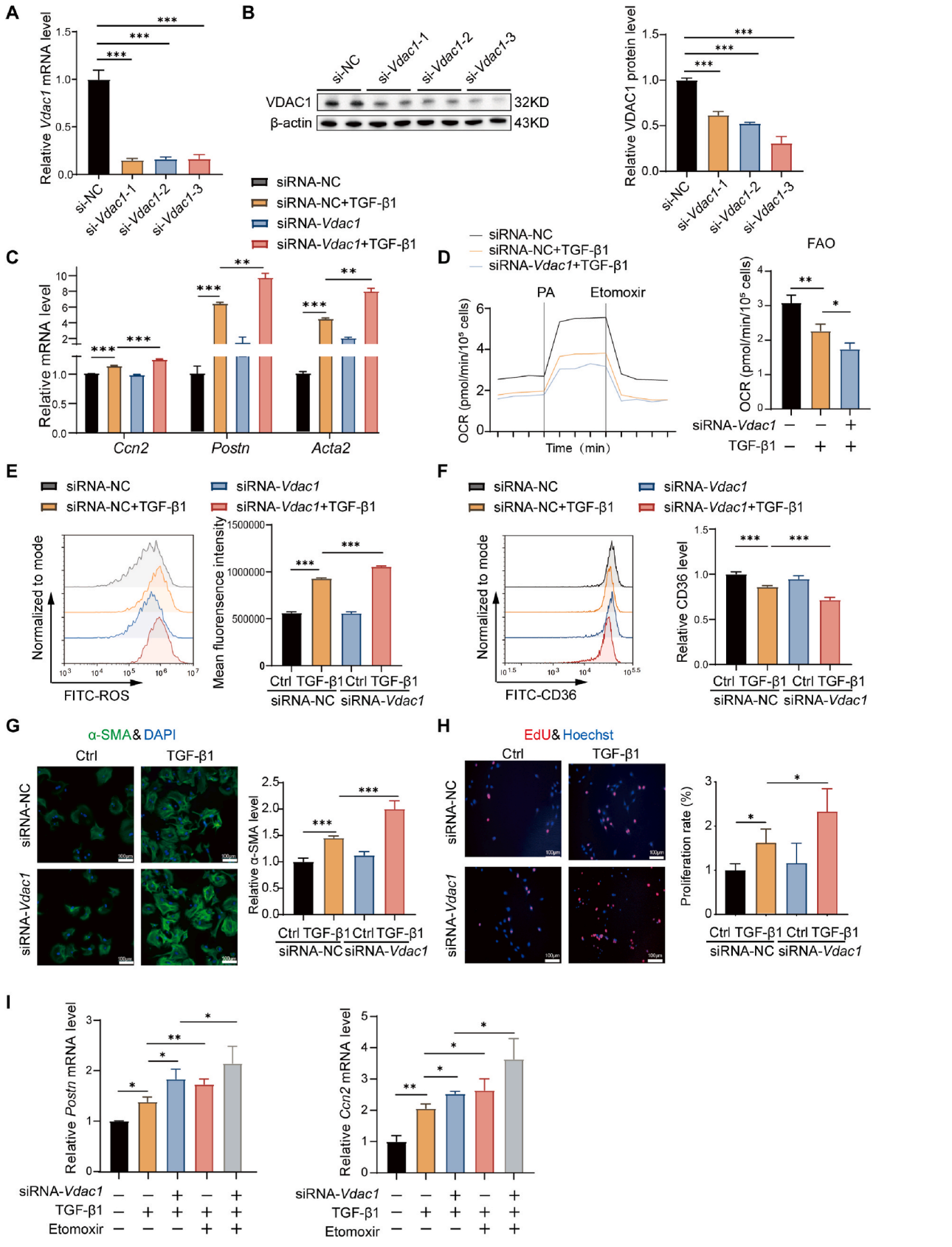

(caption on next page)

Fig. 4. Silencing VDAC1 enhances the activation of cardiac fibroblasts.
(A) Efficiency of siRNA-mediated *Vdac1* silencing of mRNA in cardiac fibroblasts (n = 3). (B) Efficiency of *Vdac1* silencing of protein in cardiac fibroblasts (n = 3). (C) mRNA levels of *Ccn2, Postn* and *Acta2* in cardiac fibroblasts with the indicated treatments, measured by RT-qPCR (n = 6). (D) Representative and statistical results of fatty acid oxidation (FAO) in primary cardiac fibroblasts treated with the Oroboros-o2k high-resolution respirometry system. OCR, oxygen consumption rate. PA, palmitic acid (n = 3). (E) ROS levels in cardiac fibroblasts treated with the indicated concentrations were detected by flow cytometry (n = 3). (F) CD36 expression in cardiac fibroblasts following the indicated treatments, as detected by flow cytometry (n = 3). (G) Immunofluorescence images showing α-SMA expression in cardiac fibroblasts. Images show staining for α-SMA (green) and the nuclei with DAPI (blue). (H) EdU staining was performed to detect cell proliferation. Cell nuclei were stained blue (Hoechst) and EdU-positive nuclei were stained red. (I) mRNA levels of *Postn* and *Ccn2* in cardiac fibroblasts after the indicated treatments, measured by RT-qPCR (n = 6). The results are presented as the means ± S.D. $*p < 0.05$, $**p < 0.01$, $***p < 0.001$; One-way ANOVA with Bonferroni *post hoc* test. (For interpretation of the references to color in this figure legend, the reader is referred to the Web version of this article.)

VDAC1 to facilitate the transport of fatty acids through the outer mitochondrial membrane. These findings indicate that VDAC1 might play a critical role as an anchoring site for CPT1a in cardiac fibroblast activation by regulating fatty acid transmembrane transport through the mitochondria. Therefore, we investigated whether VDAC1 influences the activation of cardiac fibroblasts and cardiac fibrosis.

3.3. VDAC1 expression is decreased in fibrotic cardiac tissues and TGF-β1-induced myofibroblasts

VDAC1 is one of the most abundant proteins in the outer mitochondrial membrane (OMM) and is considered to serve as a mitochondrial gatekeeper, regulating metabolic and energetic crosstalk between the mitochondria and the cytoplasm [12–16]. As RNA sequencing showed that VDAC1 might play a critical role in fatty acid transmembrane transport into the mitochondria, we tested whether VDAC1 was involved in cardiac fibroblast activation. First, we detected the expression of VDAC1 in TGF-β1-treated cardiac fibroblasts. The RT-qPCR and Western blot results showed that VDAC1 was downregulated in TGF-β1-treated CFs at both the mRNA and protein levels (Fig. 3A&B). We analyzed VDAC1 expression in a mouse model of pressure overload-induced cardiac fibrosis via TAC surgery. TAC operation-induced cardiac fibrosis was assessed by echocardiography. The IVSd and LVPWd were higher in TAC mice than in sham mice (Fig. 3C and D). TAC induced cardiac dysfunction, as shown by impaired cardiac function (EF) in TAC mice compared with sham mice (Fig. 3D). To investigate the expression of VDAC1 in cardiac fibroblasts, we sorted cardiac fibroblasts from mice in the TAC and Sham groups using flow cytometry and identified the expression of VDAC1 in $CD45^{-}CD31^{-}mEF\text{-}SK4^{+}$ cells (Fig. 3E). The results of flow cytometry analysis, RT-qPCR and Western blot assay indicated that VDAC1 expression was decreased in cardiac fibroblasts isolated from mice in the TAC group than Sham group (Fig. 3F–H). These results indicated that VDAC1 was decreased in TGF-β1-treated primary cardiac fibroblasts and cardiac fibroblasts isolated from TAC-induced fibrotic heart mice.

3.4. Silencing VDAC1 enhances the activation of cardiac fibroblasts

To explore whether VDAC1 influences FAO and how it affects FAO, we regulated the expression of VDAC1 in cardiac fibroblasts and observed the FAO intensity and the levels of FAO-associated enzymes. First, we silenced *Vdac1* with a small interfering RNA (siRNA) and confirmed the efficacy of its downregulation by RT-RT-PCR and western blotting. The results indicated that the siRNA effectively silenced *Vdac1* (Fig. 4A&B and Supplemental Fig. 3A). The sequence of si-*Vdac1*-3 was used for further experiments (Fig. 4B). Compared with the TGF-β1-treated negative control group (NC-siRNA + TGF-β1 group), silencing VDAC1 followed by TGF-β1 stimulation for 24 h (*Vdac1*-siRNA + TGF-β1 group) significantly increased the cardiac fibroblast activation markers *Ccn2, Postn* and *Acta2* (Fig. 4C). We measured the oxygen consumption rate (OCR) by Oroboros-o2k using palmitic acid (PA) as the substrate for respiration, and fatty acid oxidation was calculated as the decrease in OCR after etomoxir addition. The results indicated that VDAC1 silencing further alleviated the OCR inhibited by TGF-β1 while the substrate of respiration was PA (Fig. 4D). As fatty acid oxidation stress can induce ROS accumulation, we measured the cellular ROS levels. The results showed that VDAC1 downregulation further promoted the ROS accumulation induced by TGF-β1 (Fig. 4E). The flow cytometry assay results revealed that silencing *Vdac1* in cardiac fibroblasts further decreased the expression of CD36 compared to that of TGF-β1-treated cardiac fibroblasts (Fig. 4F). Immunofluorescence results showed that the knockdown of *Vdac1* increased the fluorescence intensity of α-SMA (Fig. 4G). EdU assay, collagen contraction assays and scratch assays also showed that silencing VDAC1 significantly enhanced the proliferation, collagen contraction and migration ability of TGF-β1-treated myofibroblasts (Fig. 4H and Supplemental Fig. 3B&C). In addition, the mRNA expression of *Postn* and *Ccn2* indicated that administration of the CPT1 inhibitor etomoxir further enhanced the activation of myofibroblasts when *Vdac1* was silenced (Fig. 4I). These results indicated that the knockdown of VDAC1 enhanced the activation of cardiac fibroblasts.

3.5. Overexpression of VDAC1 alleviates the activation of cardiac fibroblasts

The excessive accumulation of fatty acids in the cytosol can lead to oxidative stress, which is one of the key drivers offibrosis in the heart and aorta [2,30]. As LCFAs are the main fuel for FAO, their transfer into the mitochondria requires the coordination of enzymes and membrane channels [17]. VDAC1, the most abundant channel, has been proposed to mediate ionic or short-sized metabolite intermediates, including ATP, glutamate, succinate, and pyruvate, exchange between the mitochondria and cytosol. Previous studies have demonstrated that VDAC limits the ingress of respiratory substrates and modulates mitochondrial metabolism and ROS formation [31]. In our study, we hypothesized that VDAC1 plays a doorkeeper role in regulating LCFA entry into the mitochondria and that manipulating VDAC1 expression might regulate FAO and alleviate excessive oxidative stress in cardiac fibroblasts.

Overexpression of VDAC1 by infecting cardiac fibroblasts with adenovirus was confirmed at both mRNA and protein levels. (Fig. 5A&B). Compared with Ad-Ctrl + TGF-β1, Ad-*Vdac1* + TGF-β1 significantly downregulated the mRNA levels of *Postn*, *Ccn2*, and *Acta2* by qRT−PCR (Fig. 5C). The results of OCR indicated that VDAC1 overexpression enhanced the OCR inhibited by TGF-β1 while the substrate of respiration was PA (Fig. 5D). In addition, VDAC1 overexpression upregulated the levels of CD36 (Fig. 5E), whereas VDAC1 overexpression alleviated TGF-β1-induced ROS accumulation (Fig. 5F). Immunofluorescence results showed that overexpression of VDAC1 decreased α-SMA abundance (Fig. 5G). EdU, collagen contraction, and scratch assays also showed that the upregulation of VDAC1 significantly reduced the proliferation, collagen contraction, and migration ability of TGF-β1-treated myofibroblasts (Fig. 5H and Supplemental Fig. 4B&C). Additionally, etomoxir administration impaired cardiac fibroblast activation caused by VDAC1 overexpression, as shown by the mRNA expression of *Col1a1* and *Ccn2* (Fig. 5I). These results demonstrate that the regulation of VDAC1 expression affects the activation of cardiac fibroblasts, and this process might influence FAO.

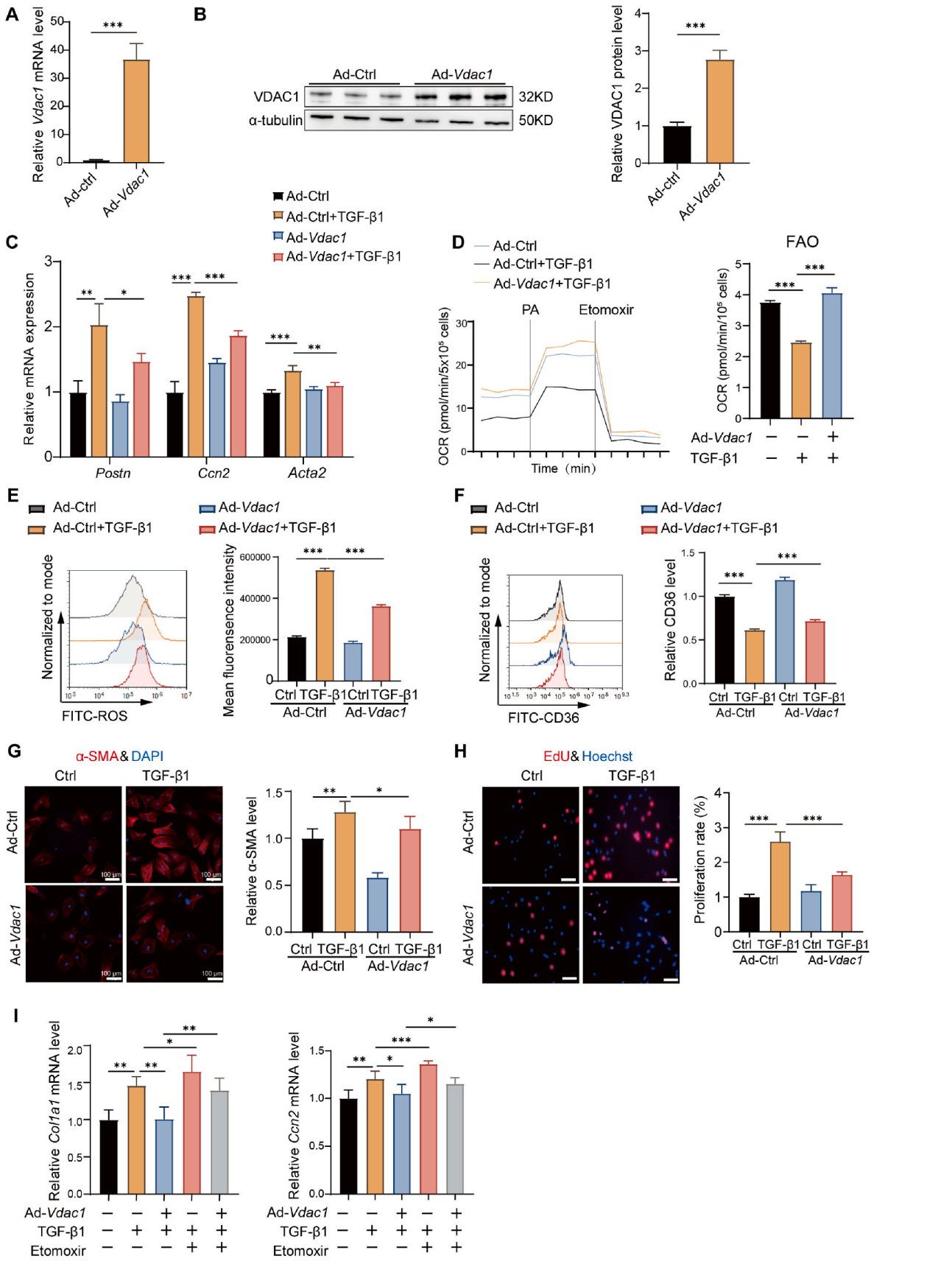

(caption on next page)

Fig. 5. Overexpression of VDAC1 alleviates the activation of cardiac fibroblasts.
(A) The efficiency of adenovirus-mediated *Vdac1* mRNA overexpression in cardiac fibroblasts (n = 3). (B) Overexpression efficiency of VDAC1 protein in cardiac fibroblasts (n = 3). (C) mRNA levels of *Ccn2, Postn* and *Acta2* in cardiac fibroblasts with the indicated treatments, measured by RT-qPCR (n = 6). (D) Representative and statistical results of fatty acid oxidation (FAO) in primary cardiac fibroblasts treated with the Oroboros-o2k high-resolution respirometry system. OCR, oxygen consumption rate. PA, palmitic acid (n = 3). (E) ROS levels in cardiac fibroblasts treated with the indicated concentrations were detected by flow cytometry (n = 3). (F) CD36 expression in cardiac fibroblasts following the indicated treatments, as detected by flow cytometry (n = 3). (G) Immunofluorescence images showing α-SMA expression in cardiac fibroblasts. Images show staining for α-SMA (green) and the nuclei with DAPI (blue). (H) EdU staining was performed to detect cell proliferation. Cell nuclei were stained blue (Hoechst) and EdU-positive nuclei were stained red. Bars represent 100 μm. (I) mRNA levels of *Col1a1* and *Ccn2* in cardiac fibroblasts after the indicated treatments, measured by RT-qPCR (n = 6). The results are presented as the means ± S.D. $*p < 0.05$, $**p < 0.01$, $***p < 0.001$; A -B, Student's *t*-test; C–I, One-way ANOVA with Bonferroni *post hoc* test. (For interpretation of the references to color in this figure legend, the reader is referred to the Web version of this article.)

3.6. Specific upregulation of VDAC1 targeting cardiac myofibroblasts alleviates TAC-induced cardiac fibrosis in mice

While the above results revealed the protective effect of VDAC1 in a cellular model of fibrogenesis, to test the function of VDAC1 *in vivo*, we constructed a pressure overload mouse model using the TAC operation. Functional studies of VDAC1 were performed by intravenously administering AAV9-*Postn*-*Vdac1* (specific overexpression of VDAC1 in *Postn*$^+$ myofibroblasts) for 7 days after TAC (Fig. 6A). The hearts of the mice in the AAV9-*Postn*-Ctrl group exhibited hypertrophy, which was alleviated by AAV9-*Postn*-*Vdac1* administration (Fig. 6B). The efficacy of AAV9 overexpression was determined in CD45$^-$CD31$^-$mEF-SK4$^+$ cardiac fibroblasts sorted from the mouse heart using flow cytometry (Fig. 6C). The results showed that the mRNA and protein levels of *Vdac1* were increased in cardiac fibroblasts sorted from mice in the AAV9-*Postn*-*Vdac1* group compared to those in the AAV9-*Postn*-Ctrl group, indicating effective transfection of AAV9 in myofibroblasts (Fig. 6C&D). To determine whether AAV9 alleviated cardiac fibroblast activation, the expression of the activation phenotype marker was detected. The results showed that overexpression of *Vdac1* in myofibroblasts decreased the mRNA level of *Acta2* (Fig. 6E). Echocardiographic analysis revealed that AAV9-*Postn*-*Vdac1* mitigated the TAC-induced cardiac hypertrophy and partially restored cardiac function (Fig. 6F). AAV9-*Postn*-Ctrl-treated mice that underwent TAC were used as controls. At 28 days after TAC, we observed a dramatic decrease in cardiac fibrosis in mice treated with AAV9-*Postn*-*Vdac1* compared to AAV9-*Postn*-Ctrl, as detected by Masson staining (Fig. 6G). In addition, AAV9-*Postn*-*Vdac1* protected against a significant recovery in the ratio of heart weight to tibial length (HW/TL) (Fig. 6H). Furthermore, the mRNA levels of fibrotic markers suggested a protective function of specific upregulation of VDAC1 in cardiac myofibroblasts (Fig. 6I).

3.7. VDAC-derived R-Tf-D-LP4 peptide alleviated pressure overload-induced cardiac functional injury and fibrosis

Finally, we explored whether VDAC1 could serve as a potential therapeutic target for the treatment of pressure overload-induced cardiac fibrosis. Three days after TAC surgery, the R-Tf-D-LP4 peptide was administered to TAC mice (10 mg/kg) via the tail vessels every three days until 4 weeks post-surgery (Fig. 7A). Vehicle-treated mice that received TAC were used as controls.

Cardiac function was assessed using echocardiography at the end of the experiment. The gross appearance of the hearts revealed that R-Tf-D-LP4 treatment reduced TAC-induced hypertrophic growth (Fig. 7B). Additionally, the R-Tf-D-LP4 peptide effectively improved cardiac function induced by pressure overload, as indicated by the maintained EF, FS, IVSd, LVPWd, and LVIDd (Fig. 7C). R-Tf-D-LP4 peptide administration partially inhibited TAC-induced cardiac hypertrophy, as shown by the decreased ratio of heart weight to tibia length (HW/TL) (Fig. 7D). Reduced interstitial collagen deposition in the heart tissue of R-Tf-D-LP4 peptide-treated mice compared to vehicle-treated mice was detected by Sirius red and Masson's trichrome staining (Fig. 7E and Supplemental Fig. 4A). Accordingly, WGA staining was performed to identify cardiac hypertrophy. R-Tf-D-LP4 peptide-treated TAC mice showed a decreased average cross-sectional area of cells compared to vehicle-treated TAC mice (Fig. 7F). HE staining showed that R-Tf-D-LP4 peptide treatment decreased cardiac hypertrophy in mice compared to that in vehicle-treated TAC mice (Fig. 7G). Moreover, the expression of fibrosis markers (*Col1a1, Postn, Ccn2*) and hypertrophy markers (*Nppa, Nppb, Myh7*) was strongly induced following TAC in vehicle-treated mice, whereas R-Tf-D-LP4 peptide treatment suppressed the expression of these markers induced by TAC (Fig. 7H). Considering the toxicity of multiple injections of the R-Tf-D-LP4 peptide, we examined the liver, kidney, and spleen by H&E staining. The results showed no significant differences in the sections of the three groups of mice under a microscope (Supplemental Figs. 4B–D). To further confirm the effect of R-Tf-D-LP4 peptide on cardiac fibroblasts, we established the TGF-β1-treated primary cardiac fibroblast activation model *in vitro*, and administrated with peptide. The RT-qPCR results indicated that the R-Tf-D-LP4 peptide effectively mitigated the cardiac fibroblast activation induced by TGF-β1 (Supplemental Fig. 4E). These results demonstrated that the R-Tf-D-LP4 peptide, as a supplementary therapy, could alleviate pressure overload-induced cardiac fibrosis and hypertrophy, which might be mediated by mitigating cardiac fibroblast activation.

4. Discussion

Metabolomics has been applied to cardiovascular diseases such as cardiac hypertrophy, fibrosis, and coronary heart disease [32–34]. Several studies have demonstrated that metabolic reprogramming plays a critical role in pressure overload-induced cardiac hypertrophy and fibrosis [35–37]. Fatty acids are responsible for the cardiomyocyte energy supply and sustained metabolic homeostasis [36,38]. Several studies have reported that excessive fatty acid accumulation or defective FAO is associated with lipotoxicity and contributes to cardiac hypertrophy and heart failure [39,40]. However, whether these metabolic abnormalities exist in cardiac fibroblasts or whether they cause fibrosis remains unclear. In this study, we performed RNA sequencing of primary cardiac fibroblasts of mice with or without TGF-β1. In myofibroblasts, degradation and oxidation of fatty acids are downregulated, whereas elongation of fatty acids is upregulated. Expression levels of genes involved in fatty acid transport, including *ACSL1*, *ACSL4*, *CPT1*, and *CPT2*. Enrichment analysis indicated that fatty acid transmembrane transport and oxidation were downregulated in TGF-β1-induced myofibroblasts. Although FAO is a complex process that depends on several enzymes, CPT1a is pivotal because of its rate-limiting role in shuttling the medium- and long-chain acyl CoA into the mitochondrial matrix for oxidation [41]. We analyzed the LC-MS/MS results of the LCFA spectrum, which indicated that middle- and long-chain FAs accumulated in myofibroblasts. The accumulation of middle-chain acylcarnitines may result from incomplete FAO of LCFAs [42]. In addition, excess fatty acid accumulation has been observed in TGF-β1-treated cardiac fibroblasts and has been proposed to induce ROS in myofibroblasts.

LCFAs are the basic fuel for oxidation in the heart to meet the high ATP demand of a constant heartbeat [43]. During cardiac remodeling, metabolic phenotype changes, such as proportionally high use of fatty acids shift into glucose and its β-oxidation decreases [44,45]. FAO supplies 70% of the ATP in the physiological state, and CPT1a, a

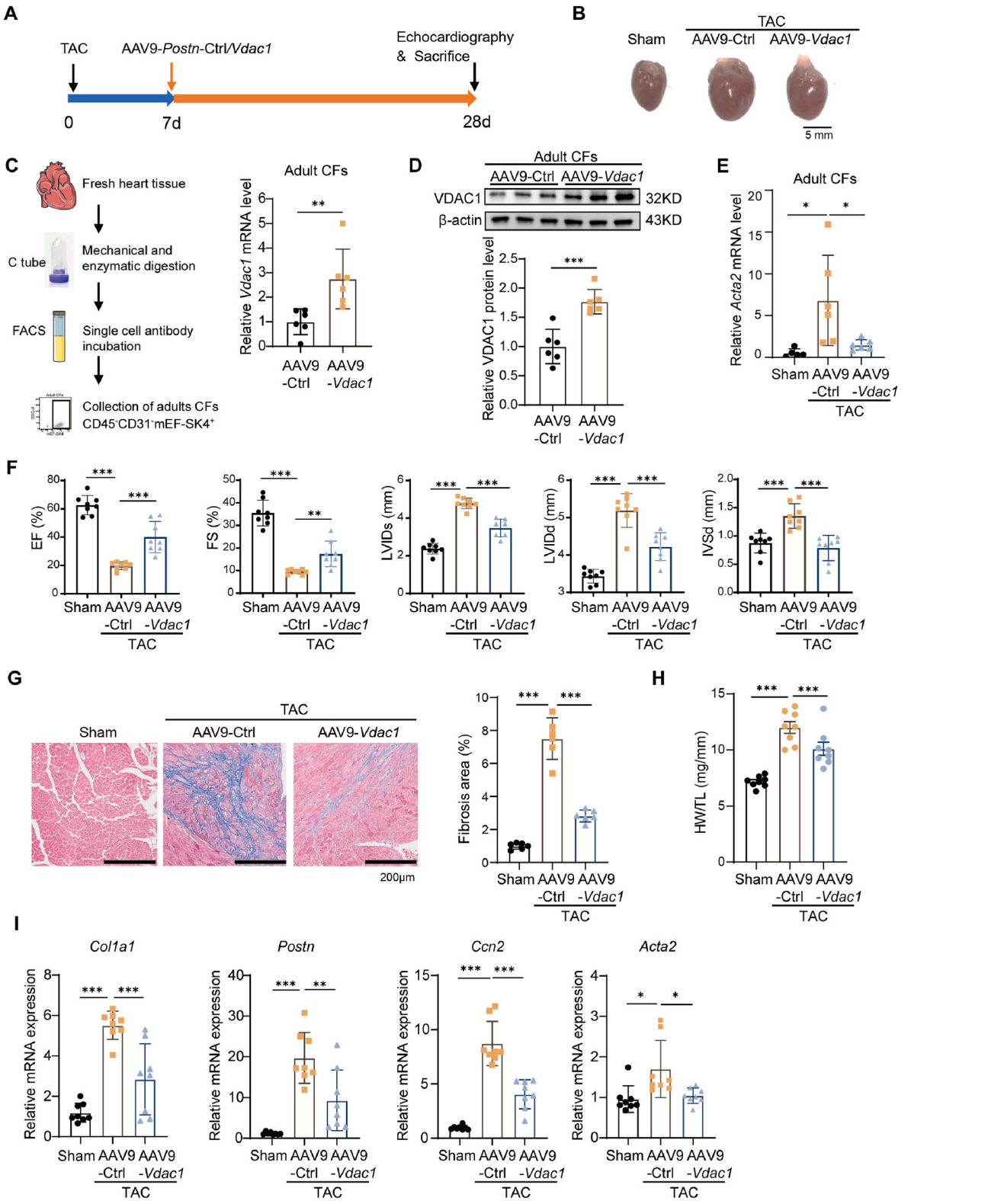

Fig. 6. Fibroblast-specific upregulation of VDAC1 expression alleviates TAC-induced cardiac fibrosis in mice.
(A) Schematic diagram outlining the *in vivo* experiments. Mice were treated with AAV9-*Postn*-*Vdac1*/Ctrl (AAV9-*Vdac1*/Ctrl) at 7 days after TAC operation. (B) The gross appearance of the hearts obtained from the mice. (C) Specific *Vdac1* mRNA overexpression efficiency of AAV9-*Vdac1* in cardiac fibroblasts of TAC-operated mice, as detected using RT-qPCR (n = 6). (D) Specific VDAC1 protein overexpression efficiency of AAV9-*Vdac1* in cardiac fibroblasts of TAC-operated mice, as detected using western blotting (n = 6). (E) mRNA levels of *Acta2* in cardiac fibroblast in TAC-operated mice (n = 6). (F) Cardiac function indicators measured using echocardiography (EF, FS, LVIDd, LVIDs and IVSd) in mice 3 weeks after tail vein injection of AAV9-*Vdac1*. (G) Representative image of Masson staining and the statistical results of fibrosis of hearts from mice with the indicated treatment. (H) The anatomy index, HW/TL of mice with indicated treatment. (I) mRNA levels of the fibrotic markers, *Col1a1, Postn, Ccn2,* and *Acta2* in CFs with the indicated treatment measured using qRT−PCR (n = 6). The results are presented as the means ± S.D. *$p < 0.05$, **$p < 0.01$, ***$p < 0.001$; C&D, Student's *t*-test; E-I, One-way ANOVA with Bonferroni *post hoc* test.

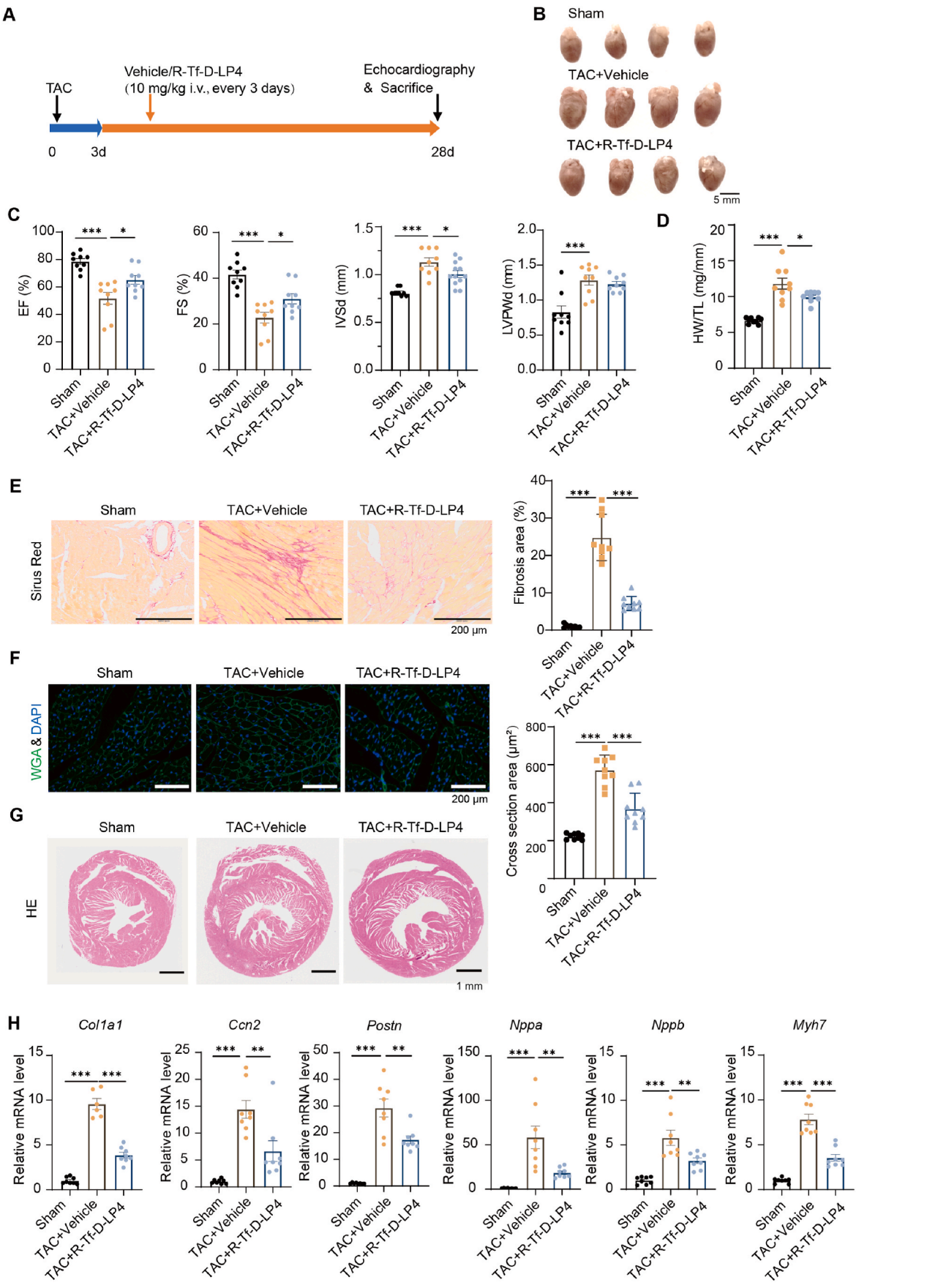

(caption on next page)

Fig. 7. VDAC-derived R-Tf-D-LP4 peptide alleviates pressure overload-induced cardiac dysfunction and fibrosis.
(A) Schematic of *in vivo* experiments. Mice were treated with the R-Tf-D-LP4 peptide 3 days after TAC, followed by treatment every 3 days. (B) Gross appearance of the hearts obtained from mice. (C) Cardiac function indicators measured by echocardiography (EF, FS, LVIDd, LVIDs, and IVSd) in mice 4 weeks after TAC. (D) Anatomical index (HW/TL) of mice subjected to the indicated treatments. (E) Representative images of Sirius red staining in mice subjected to the indicated treatments. (F) Representative images of the immunofluorescence staining of WGA in mice with the indicated treatments. (G) Representative images of HE staining of mice subjected to the indicated treatments. (H) mRNA levels of fibrotic markers (*Col1a1, Postn, Ccn2*) and hypertrophic markers (*Nppa, Nppb, Myh7*) in the hearts of mice with the indicated treatments, measured by RT-qPCR (n = 6–9). The results are presented as the means ± S.D. $*p < 0.05$, $**p < 0.01$, $***p < 0.001$; One-way ANOVA with Bonferroni *post hoc* test. (For interpretation of the references to color in this figure legend, the reader is referred to the Web version of this article.)

rate-limiting enzyme, is considered a targetable enzyme. Previous studies have shown that CPT1a is decreased in pathological states, and CPT1a overexpression alleviates tissue fibrosis in the kidney, liver, and lungs [46,47]. In accordance with our study, suppression of FAO by inhibiting CPT1 activity with etomoxir increased myofibroblast parameters, whereas enhancement of FAO by activating AMPK with AICAR resulted in the protection of fibroblast activation. As substrates in the transport process, restrict the activity of CPT1a [48]. Angelini et al. reported that the loss of PHD2/3 led to an accumulation of LCFAs in mouse hearts, whereas CPT1b protein levels did not differ. Therefore, the downstream of CPT1b might be more easily affected by the LCFA concentration. Long-chain acyl-CoA esters are converted to acyl-carnitine esters by CPT1a and then transported into the mitochondrial intermembrane space via channel proteins [49]. VDAC1 is the most abundant channel protein on the OMM and is connected to the cytosol and mitochondrial intermembrane space. In mouse steatosis and NASH models, the CPT1/VDAC1/ACSL complex is considered to be the transporter of LCFA-CoA, whereas VDAC1 acts as the gatekeeper for the passage of FAO substrates [18].

Several studies have confirmed the crucial role of VDAC1 in the regulation of mitochondrial function, apoptosis, and metabolic homeostasis [50]. VDAC1 is a multifunctional channel protein that modulates the cellular metabolism. VDAC1 transfers several metabolites including pyruvate, malonate, and nucleotides [51]. VDAC1 also regulates cholesterol transport, Ca^{2+} signal transduction, and mtDNA release [52–54]. In this study, VDAC1 was assessed to determine whether it functions as a channel for long-chain fatty acylcarnitines and plays a protective role against cardiac fibroblast activation and fibrosis. TAC *in vivo* and TGF-β1 treatment *in vitro* decreased the expression of VDAC1 at both the mRNA and protein levels. In vitro, silencing and overexpression of VDAC1 revealed that VDAC1 plays a protective role in the activation of cardiac fibroblasts in terms of proliferation, metabolism, and profibrotic protein secretion. Additionally, the upregulation of VDAC1 decreased ROS production and enhanced FAO intensity. Specific overexpression of VDAC1 in myofibroblasts using AAV9-*Postn*-vadc1, which contained a periostin promoter, was used to determine the role of VDAC1 in cardiac fibrosis. Consistent with the *in vitro* results, *in vivo* results confirmed the protective capacity of VDAC1 in alleviating cardiac fibrosis. Loss of VDAC1 may cause mitochondria to stop oxidizing fatty acids, and VDAC1 inhibitors can inhibit palmitate oxidation [18].

Although there are several drugs targeting fatty acid metabolism for fibrotic diseases, treatments targeting cardiac fibroblast metabolic dysregulation in cardiac diseases are lacking. R-Tf-D-LP4, a VDAC1-derived peptide, has been shown to enhance catabolic capacity and promote fatty acid transfer into mitochondria and fatty acid oxidation by upregulating the expression of enzymes involved in fatty acid oxidation and transportation in NASH and a steatohepatitis mouse model [18]. In addition, the R-Tf-D-LP4 peptide alleviates streptozotocin and high-fat diet 32-induced type 2 diabetes by decreasing glucose levels and promoting β-cell proliferation in obese mice [55]. Consistent with previous studies, our research revealed that R-Tf-D-LP4 alleviated cardiac fibrosis induced by TAC and elevated cardiac function. HE staining of other organs, including the kidney, liver, and spleen, indicated that systemic administration of R-Tf-D-LP4 had no significant toxicity. Unfortunately, we cannot rule out the effect of R-Tf-D-LP4 on other cells such as cardiomyocytes, endothelial cells, and immune cells. To validate the effects of R-Tf-D-LP4 on cardiac fibroblasts, we established an *in vitro* fibroblast activation model and administered R-Tf-D-LP4. RT-qPCR confirmed that R-Tf-D-LP4 attenuated CF activation of cardiac fibroblasts. Overexpression of VDAC1 in activated fibroblasts has been confirmed to alleviate cardiac fibrosis through AAV9-*Postn-Vdac1* to specifically overexpress VDAC1 in myofibroblasts. As an alternative therapeutic approach, the peptide R-Tf-D-LP4 demonstrated slightly reduced specificity, but still achieved significant alleviation of cardiac fibrosis.

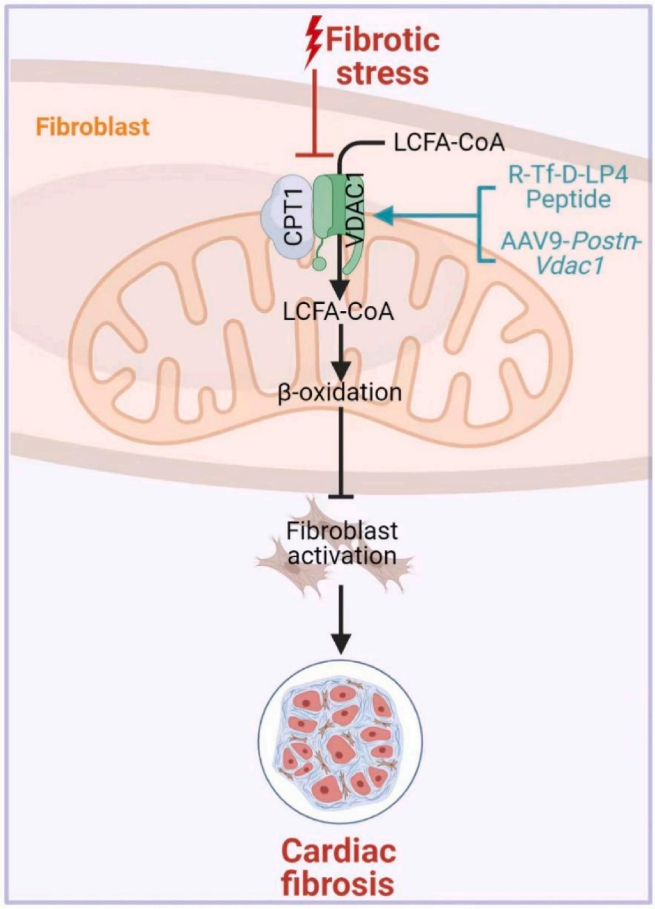

Fig. 8. A diagram outlining the mechanism of VDAC1 in cardiac fibrosis.
Under fibrotic stress, such as pressure overload and TGF-β1, downregulated VDAC1 failed to form a complex with CPT1, thereby hindering the entry of long-chain fatty acids (LCFAs) into mitochondria for β-oxidation. Furthermore, metabolic alterations in cardiac fibroblasts lead to their continuous activation, which exacerbates cardiac fibrosis and function. The administration of VDAC1-derived R-Tf-D-LP4 peptides or specific overexpression of VDAC1 in myofibroblasts inhibited fibroblast activation and alleviated pressure overload-induced cardiac fibrosis.

To our knowledge, this is the first study to demonstrate the preventive role of VDAC1 in the regulation of fatty acid metabolism in cardiac fibroblasts. This study suggests that metabolic regulation may be an effective treatment for cardiac fibrotic diseases. Our study suggests that the downregulation of FAO contributes to cardiac fibroblast activation, and this process may be caused by the accumulation of LCFAs in

the cytosol, with hindered transfer into the mitochondria. Overexpression of the mitochondrial gatekeeper VDAC1 alleviates myofibroblast phenotypes and increases FAO levels. Specific overexpression of VDAC1 in myofibroblasts under the control of the periostin promoter prevents pressure overload-induced cardiac fibrosis and enhances cardiac function. In addition, systemic administration of the VDAC1-derived peptide R-Tf-D-LP4 exerted a function similar to that of the specific overexpression of AAV in mouse models (Fig. 8). However, the mechanism through which VDAC1 regulates FAO is not well understood.

5. Conclusion

In summary, we described the LCFA spectrum and metabolic alterations in myofibroblast activation, and investigated the role of the gatekeeper VDAC1 in regulating cardiac fibroblast activation. FAO is a potential target for the treatment of cardiac fibrosis, and the R-Tf-D-LP4 peptide may be a promising agent for alleviating cardiac fibrosis by targeting VDAC1.

Authors' contributions

XT and XL designed and supervised the whole project. GT and JZ performed the experiments and collected the data and drafted the manuscript. YQ, JZ, QK, and JL designed the statistical analysis strategy and performed the statistical analyses. GT, JZ, YQ, QK, JL, YX, WW, XT, and XL contributed to the discussion. GT, JZ, XT, and XL edited the manuscript. All of the authors reviewed and approved the final version of the manuscript.

Funding

This study was funded by the National Natural Science Foundation of China (12072215, 81970426, and 12202386), Science and Technology Department of Sichuan Province (2023NSFSC1640), China Postdoctoral Science Foundation (2022M722278), and Chunhui Program of Ministry of Education of China (HZKY20220573).

Declaration of competing interest

The authors declare that the research was conducted in the absence of any commercial or financial relationships that could be construed as a potential conflict of interest.

Data availability

Data will be made available on request.

Appendix A. Supplementary data

Supplementary data to this article can be found online at https://doi.org/10.1016/j.redox.2023.102907.

References

[1] N.G. Frangogiannis, Cardiac fibrosis: cell biological mechanisms, molecular pathways and therapeutic opportunities, Mol. Aspect. Med. 65 (2019) 70–99.
[2] N.G. Frangogiannis, Cardiac fibrosis, Cardiovasc. Res. 117 (2021) 1450–1488.
[3] Y. Chen, J. Zhou, Z. Wei, Y. Cheng, G. Tian, Y. Quan, Q. Kong, W. Wu, X. Liu, Identification of circular RNAs in cardiac hypertrophy and cardiac fibrosis, Front. Pharmacol. 13 (2022), 940768.
[4] J. Zhou, G. Tian, Y. Quan, Q. Kong, F. Huang, J. Li, W. Wu, Y. Tang, Z. Zhou, X. Liu, The long noncoding RNA THBS1-AS1 promotes cardiac fibroblast activation in cardiac fibrosis by regulating TGFBR1, JCI Insight 8 (2023), e160745.
[5] Q. Kong, J. Zhou, C. Ma, Z. Wei, Y. Chen, Y. Cheng, W. Wu, Z. Zhou, Y. Tang, X. Liu, Inhibition of long noncoding RNA Gm41724 alleviates pressure overload-induced cardiac fibrosis by regulating lamina-associated polypeptide 2α, Pharmacol. Res. 188 (2023), 106677.
[6] I. Russo, M. Cavalera, S. Huang, Y. Su, A. Hanna, B. Chen, A.V. Shinde, S. J. Conway, J. Graff, N.G. Frangogiannis, Protective effects of activated myofibroblasts in the pressure-overloaded myocardium are mediated through smad-dependent activation of a matrix-preserving program, Circ. Res. 124 (2019) 1214–1227.
[7] X. Sun, Y. Zhang, X.-F. Chen, X. Tang, Acylations in cardiovascular biology and diseases, what's beyond acetylation, EBioMedicine 67 (2023), 104418.
[8] X. Tang, X.F. Chen, H.Z. Chen, D.P. Liu, Mitochondrial Sirtuins in cardiometabolic diseases, Clin. Sci. 131 (2017) 2063–2078.
[9] M. Pesce, G.N. Duda, G. Forte, H. Girao, A. Raya, P. Roca-Cusachs, J.P.G. Sluijter, C. Tschope, S. Van Linthout, Cardiac fibroblasts and mechanosensation in heart development, health and disease, Nat. Rev. Cardiol. 20 (2023) 309–324.
[10] D. Montaigne, L. Butruille, B. Staels, PPAR control of metabolism and cardiovascular functions, Nat. Rev. Cardiol. 18 (2021) 809–823.
[11] L. He, T. Kim, Q. Long, J. Liu, P. Wang, Y. Zhou, Y. Ding, J. Prasain, P.A. Wood, Q. Yang, Carnitine palmitoyltransferase-1b deficiency aggravates pressure overload-induced cardiac hypertrophy caused by lipotoxicity, Circulation 126 (2012) 1705–1716.
[12] V. Shoshan-Barmatz, E.N. Maldonado, Y. Krelin, VDAC1 at the crossroads of cell metabolism, apoptosis and cell stress, Cell Stress 1 (2017) 11–36.
[13] N.N. Wu, Y. Bi, A. Ajoolabady, F. You, J. Sowers, Q. Wang, A.F. Ceylan, Y. Zhang, J. Ren, Parkin insufficiency accentuates high-fat diet-induced cardiac remodeling and contractile dysfunction through VDAC1-mediated mitochondrial Ca(2+) overload, JACC Basic Transl. Sci. 7 (2022) 779–796.
[14] N.N. Wu, L. Wang, X. Xu, G.D. Lopaschuk, Y. Zhang, J. Ren, Site-specific ubiquitination of VDAC1 restricts its oligomerization and mitochondrial DNA release in liver fibrosis, Exp. Mol. Med. 55 (2023) 269–280.
[15] H. Zhou, Z. Dai, J. Li, J. Wang, H. Zhu, X. Chang, Y. Wang, TMBIM6 prevents VDAC1 multimerization and improves mitochondrial quality control to reduce sepsis-related myocardial injury, Metabolism 140 (2023), 155383.
[16] P. Salin Raj, A. Nair, M.R. Preetha Rani, K. Rajankutty, S. Ranjith, K.G. Raghu, Ferulic acid attenuates high glucose-induced MAM alterations via PACS2/IP3R2/FUNDC1/VDAC1 pathway activating proapoptotic proteins and ameliorates cardiomyopathy in diabetic rats, Int. J. Cardiol. 372 (2023) 101–109.
[17] A. Angelini, P.K. Saha, A. Jain, S.Y. Jung, R.L. Mynatt, X. Pi, L. Xie, PHDs/CPT1B/VDAC1 axis regulates long-chain fatty acid oxidation in cardiomyocytes, Cell Rep. 37 (2021), 109767.
[18] S. Pittala, Y. Krelin, Y. Kuperman, V. Shoshan-Barmatz, A mitochondrial VDAC1-based peptide greatly suppresses steatosis and NASH-associated pathologies in a mouse model, Mol. Ther. 27 (2019) 1848–1862.
[19] J. Zhou, G. Tian, Y. Quan, J. Li, X. Wang, W. Wu, M. Li, X. Liu, Inhibition of P2X7 purinergic receptor ameliorates cardiac fibrosis by suppressing NLRP3/IL-1beta pathway, Oxid. Med. Cell. Longev. 2020 (2020), 7956274.
[20] M.I. Love, W. Huber, S. Anders, Moderated estimation of fold change and dispersion for RNA-seq data with DESeq2, Genome Biol. 15 (2014) 550.
[21] S. Hwang, K.W. Chung, Targeting fatty acid metabolism for fibrotic disorders, Arch Pharm. Res. (Seoul) 44 (2021) 839–856.
[22] P.R. Gajjala, R.K. Kasam, D. Soundararajan, D. Sinner, S.K. Huang, A.G. Jegga, S. K. Madala, Dysregulated overexpression of Sox9 induces fibroblast activation in pulmonary fibrosis, JCI Insight (2021) 6.
[23] S. Uchinomiya, N. Matsunaga, K. Kamoda, R. Kawagoe, A. Tsuruta, S. Ohdo, A. Ojida, Fluorescence detection of metabolic activity of the fatty acid beta oxidation pathway in living cells, Chem. Commun. (Camb.) 56 (2020) 3023–3026.
[24] H. Shu, Y. Peng, W. Hang, J. Nie, N. Zhou, D.W. Wang, The role of CD36 in cardiovascular disease, Cardiovasc. Res. 118 (2022) 115–129.
[25] L. Jin, L. Geng, L. Ying, L. Shu, K. Ye, R. Yang, Y. Liu, Y. Wang, Y. Cai, X. Jiang, Q. Wang, X. Yan, B. Liao, J. Liu, F. Duan, G. Sweeney, C.W.H. Woo, Y. Wang, Z. Xia, Q. Lian, A. Xu, FGF21-Sirtuin 3 Axis confers the protective effects of exercise against diabetic cardiomyopathy by governing mitochondrial integrity, Circulation 146 (2022) 1537–1557.
[26] T. Tian, Y. Lu, J. Lin, M. Chen, H. Qiu, W. Zhu, H. Sun, J. Huang, H. Yang, W. Deng, CPT1A promotes anoikis resistance in esophageal squamous cell carcinoma via redox homeostasis, Redox Biol. 58 (2022), 102544.
[27] H. Gong, H. Chen, P. Xiao, N. Huang, X. Han, J. Zhang, Y. Yang, T. Li, T. Zhao, H. Tai, W. Xu, G. Zhang, C. Gong, M. Yang, X. Tang, H. Xiao, miR-146a impedes the anti-aging effect of AMPK via NAMPT suppression and NAD^+/SIRT inactivation, Signal Transduct. Targeted Ther. 7 (2022) 66.
[28] X. Tang, X.F. Chen, N.Y. Wang, X.M. Wang, S.T. Liang, W. Zheng, Y.B. Lu, X. Zhao, D.L. Hao, Z.Q. Zhang, M.H. Zou, D.P. Liu, H.Z. Chen, SIRT2 acts as a cardioprotective deacetylase in pathological cardiac hypertrophy, Circulation 136 (2017) 2051–2067.
[29] K. Lee, J. Kerner, C.L. Hoppel, Mitochondrial carnitine palmitoyltransferase 1a (CPT1a) is part of an outer membrane fatty acid transfer complex, J. Biol. Chem. 286 (2011) 25655–25662.
[30] Y. Zhang, X. Wang, X.-K. Li, S.-J. Lv, H.-P. Wang, Y. Liu, J. Zhou, H. Gong, X.-F. Chen, S.-C. Ren, H. Zhang, Y. Dai, H. Cai, B. Yan, H.-Z. Chen, X. Tang, Sirtuin 2 deficiency aggravates ageing-induced vascular remodelling in humans and mice, Eur. Heart J. 44 (2023) 2746–2759.
[31] E.N. Maldonado, VDAC-tubulin, an anti-warburg pro-oxidant switch, Front. Oncol. 7 (2017) 4.
[32] S. Ranjbarvaziri, K.B. Kooiker, M. Ellenberger, G. Fajardo, M. Zhao, A.S. Vander Roest, R.A. Woldeyes, T.T. Koyano, R. Fong, N. Ma, L. Tian, G.M. Traber, F. Chan, J. Perrino, S. Reddy, W. Chiu, J.C. Wu, J.Y. Woo, K.M. Ruppel, J.A. Spudich, M. P. Snyder, K. Contrepois, D. Bernstein, Altered cardiac energetics and mitochondrial dysfunction in hypertrophic cardiomyopathy, Circulation 144 (2021) 1714–1731.
[33] Y. Fan, Y. Li, Y. Chen, Y.J. Zhao, L.W. Liu, J. Li, S.L. Wang, R.N. Alolga, Y. Yin, X. M. Wang, D.S. Zhao, J.H. Shen, F.Q. Meng, X. Zhou, H. Xu, G.P. He, M.D. Lai, P. Li,

W. Zhu, L.W. Qi, Comprehensive metabolomic characterization of coronary artery diseases, J. Am. Coll. Cardiol. 68 (2016) 1281–1293.
[34] R.W. McGarrah, S.B. Crown, G.F. Zhang, S.H. Shah, C.B. Newgard, Cardiovascular metabolomics, Circ. Res. 122 (2018) 1238–1258.
[35] J. Ritterhoff, S. Young, O. Villet, D. Shao, F.C. Neto, L.F. Bettcher, Y.A. Hsu, S. C. Kolwicz Jr., D. Raftery, R. Tian, Metabolic remodeling promotes cardiac hypertrophy by directing glucose to aspartate biosynthesis, Circ. Res. 126 (2020) 182–196.
[36] J. Ritterhoff, T.S. McMillen, O. Villet, S. Young, S.C. Kolwicz Jr., T. Senn, A. Caudal, R. Tian, Increasing fatty acid oxidation elicits a sex-dependent response in failing mouse hearts, J. Mol. Cell. Cardiol. 158 (2021) 1–10.
[37] D. Banerjee, R. Datta Chaudhuri, S. Niyogi, S. Roy Chowdhuri, M. Poddar Sarkar, R. Chatterjee, P. Chakrabarti, S. Sarkar, Metabolic impairment in response to early induction of C/EBPβ leads to compromised cardiac function during pathological hypertrophy, J. Mol. Cell. Cardiol. 139 (2020) 148–163.
[38] S. Gao, G. Li, Y. Shao, Z. Wei, S. Huang, F. Qi, Y. Jiao, Y. Li, C. Zhang, J. Du, FABP5 deficiency impairs mitochondrial function and aggravates pathological cardiac remodeling and dysfunction, Cardiovasc. Toxicol. 21 (2021) 619–629.
[39] J.R. Goldenberg, A.N. Carley, R. Ji, X. Zhang, M. Fasano, P.C. Schulze, E. D. Lewandowski, Preservation of acyl coenzyme A attenuates pathological and metabolic cardiac remodeling through selective lipid trafficking, Circulation 139 (2019) 2765–2777.
[40] H. Moriyama, J. Endo, H. Ikura, H. Kitakata, M. Momoi, Y. Shinya, S. Ko, G. Ichihara, T. Hiraide, K. Shirakawa, A. Anzai, Y. Katsumata, M. Sano, Qualitative and quantitative effects of fatty acids involved in heart diseases, Metabolites 12 (2022) 210.
[41] I.R. Schlaepfer, M. Joshi, CPT1A-mediated fat oxidation, mechanisms, and therapeutic potential, Endocrinology 161 (2020) bqz046.
[42] S.H. Adams, C.L. Hoppel, K.H. Lok, L. Zhao, S.W. Wong, P.E. Minkler, D.H. Hwang, J.W. Newman, W.T. Garvey, Plasma acylcarnitine profiles suggest incomplete long-chain fatty acid beta-oxidation and altered tricarboxylic acid cycle activity in type 2 diabetic African-American women, J. Nutr. 139 (2009) 1073–1081.
[43] A.N. Carley, H. Taegtmeyer, E.D. Lewandowski, Matrix revisited: mechanisms linking energy substrate metabolism to the function of the heart, Circ. Res. 114 (2014) 717–729.
[44] R. Lahey, X. Wang, A.N. Carley, E.D. Lewandowski, Dietary fat supply to failing hearts determines dynamic lipid signaling for nuclear receptor activation and oxidation of stored triglyceride, Circulation 130 (2014) 1790–1799.
[45] J.M. O'Donnell, A.D. Fields, N. Sorokina, E.D. Lewandowski, The absence of endogenous lipid oxidation in early stage heart failure exposes limits in lipid storage and turnover, J. Mol. Cell. Cardiol. 44 (2008) 315–322.
[46] V. Miguel, J. Tituana, J.I. Herrero, L. Herrero, D. Serra, P. Cuevas, C. Barbas, D. R. Puyol, L. Marquez-Exposito, M. Ruiz-Ortega, C. Castillo, X. Sheng, K. Susztak, M. Ruiz-Canela, J. Salas-Salvado, M.A.M. Gonzalez, S. Ortega, R. Ramos, S. Lamas, Renal tubule Cpt1a overexpression protects from kidney fibrosis by restoring mitochondrial homeostasis, J. Clin. Invest. 131 (2021), e140695.
[47] Z. Wang, L. Chen, Y. Huang, M. Luo, H. Wang, Z. Jiang, J. Zheng, Z. Yang, Z. Chen, C. Zhang, L. Long, Y. Wang, X. Li, F. Liao, Y. Gan, P. Luo, Y. Liu, Y. Wang, XuTan, Z. Zhou, A. Zhang, C. Shi, Pharmaceutical targeting of succinate dehydrogenase in fibroblasts controls bleomycin-induced lung fibrosis, Redox Biol. 46 (2021), 102082.
[48] A.S. Divakaruni, W.Y. Hsieh, L. Minarrieta, T.N. Duong, K.K.O. Kim, B.R. Desousa, A.Y. Andreyev, C.E. Bowman, K. Caradonna, B.P. Dranka, D.A. Ferrick, M. Liesa, L. Stiles, G.W. Rogers, D. Braas, T.P. Ciaraldi, M.J. Wolfgang, T. Sparwasser, L. Berod, S.J. Bensinger, A.N. Murphy, Etomoxir inhibits macrophage polarization by disrupting CoA homeostasis, Cell Metabol. 28 (2018) 490–503.e497.
[49] D. Neess, S. Bek, H. Engelsby, S.F. Gallego, N.J. Færgeman, Long-chain acyl-CoA esters in metabolism and signaling: role of acyl-CoA binding proteins, Prog. Lipid Res. 59 (2015) 1–25.
[50] A.K.S. Camara, Y. Zhou, P.C. Wen, E. Tajkhorshid, W.M. Kwok, Mitochondrial VDAC1: a key gatekeeper as potential therapeutic target, Front. Physiol. 8 (2017) 460.
[51] S.J. Ham, D. Lee, H. Yoo, K. Jun, H. Shin, J. Chung, Decision between mitophagy and apoptosis by Parkin via VDAC1 ubiquitination, Proc. Natl. Acad. Sci. U.S.A. 117 (2020) 4281–4291.
[52] H. Huang, X. Hu, C.O. Eno, G. Zhao, C. Li, C. White, An interaction between Bcl-xL and the voltage-dependent anion channel (VDAC) promotes mitochondrial Ca2+ uptake, J. Biol. Chem. 288 (2013) 19870–19881.
[53] J. Kim, R. Gupta, L.P. Blanco, S. Yang, A. Shteinfer-Kuzmine, K. Wang, J. Zhu, H. E. Yoon, X. Wang, M. Kerkhofs, H. Kang, A.L. Brown, S.J. Park, X. Xu, E. Zandee van Rilland, M.K. Kim, J.I. Cohen, M.J. Kaplan, V. Shoshan-Barmatz, J.H. Chung, VDAC oligomers form mitochondrial pores to release mtDNA fragments and promote lupus-like disease, Science 366 (2019) 1531–1536.
[54] Y.-N. Ding, X. Tang, Sensing mitochondrial DNA stress in cardiotoxicity, Trends Endocrinol. Metabol. 34 (2023) 1–3.
[55] S. Pittala, I. Levy, S. De, S. Kumar Pandey, N. Melnikov, T. Hyman, V. Shoshan-Barmatz, The VDAC1-based R-Tf-D-LP4 peptide as a potential treatment for diabetes mellitus, Cells 9 (2020) 481.